CAPZEO-2014
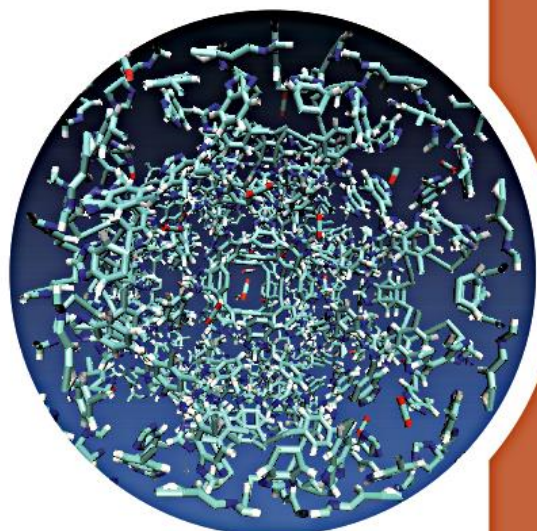
INTERNATIONAL SUMMER SCHOOL ON QUANTUM ELECTRONIC CALCULATIONS, THEORETICAL METHODS FOR MICROSCOPIC DYNAMICAL STUDIES

Université Mohammed V-Agdal
Faculté des Sciences
Rabat

LS3ME
Spectroscopie, Modélisation Moléculaire, Matériaux et Environnement

Chair: Prof. N.Komiha
(University Mohammed V-Agdal, Rabat,Morocco)

Scientific organizing committee

Prof. H.Abou El Makarim(Morocco)
Prof.D. Benoit (UK),
Prof. D. Borgis (France)
Prof. G. Chambaud (France),
Dr. F.X. Coudert (France).
Prof.M. Hochlaf (France)
Dr. R. Linguerri (France) ,
Prof. O. K.Kabbaj (Morrocco),
Prof.K.Marakchi(Morocco)
Prof. M. L. Senent (Spain)
Prof.V. Timon (Spain)

9–12 June 2014
FACULTY OF SCIENCE OF RABAT – UNIVERSITY MOHAMMED V–AGDAL
Laboratory LS3ME– Theoretical Chemistry & European Project CapZeo

UNIVERSITY OF Hull

CONSEJO SUPERIOR DE INVESTIGACIONES CIENTÍFICAS

Le groupement d'assurances du supérieur

UPEM

www.fsr.ac.ma/ancien/index.php/congres.html

Preface

This international summer school is organized in the context of CapZeo project

Marie Curie Action IRSES-CAPZEO

FP7-PEOPLE-2012-IRSES

IRSES-CAPZEO, International Research Staff Exchange Scheme, is a new Marie Curie Action, launched in October 2012. The duration of this project is 4 years.

The project aims to strengthen research partnerships between European research organizations and non-European research organizations from countries with which the EC has an S&T agreement, through staff exchange and networking activities. Participants are non-profit public or private research organisations which receive support from the EC to establish or reinforce long-term cooperation with third country research organizations.

The subject of this project concerns the CO_2 capture and storage by nanoporous materials like Zeolite Imidazole Frameworks (ZIFs). The state of art of the theoretical quantum methods will be developed and applied for the microscopic aspects study.

The project has four partners, 3 from Europe (University of Marne La Vallée, France, Instituto de Estructura de la Materia, CSIC, Spain and the University of Hull, United Kingdom) and one from Morocco (University Mohammed V-Agdal). This project has 4 work packages. The first was held last September in Marne La Vallée: an international symposium on CO_2 capture, and this summer school is the second work package.

Introduction

The school will focus on introduction of theoretical methods for the treatment of small, medium sized and large systems, long range interactions and molecule-surface interfaces. With the fast development of computer sciences, theoretical methods represent an efficient instrument for the study of systems involving molecular species. Advanced computational electronic structure methods have become a practical tool for non-specialists in both university and industry, and this school will provide experience in their use.

A wide range of methods, from standard density functional theory to highly sophisticated local and explicitly-correlated coupled-cluster methods, and their applications in spectroscopy, environment and thermochemistry will be covered. In addition, the simulation of complex systems and the treatment of solid-state and interfaces methods will also be presented. For each subject, an introductory lecture will be given, followed by computer exercises, mainly using the GAUSSIAN and MOLPRO quantum chemistry package and the MATERIAL STUDIO and CP2K codes. Basic knowledge of quantum mechanics, quantum chemistry and mathematical tools is required.

English will be the official language of the school, however, translations in French will be provided if necessary.

Participants will be invited to present their research results in the field of experimental, theoretical and computational chemistry in the form of posters.

The school will last four days where participants in the CapZeo project will give lectures and selected invited speakers may also help by presenting additional lectures. All of them will participate to the computer exercises sessions.

Each day will be especially dedicated to different fields:

a) The two first sessions will be dedicated to the basic quantum chemistry methods, and most popular correlated methods for the treatment of the isolated molecules; applications for chemical reactivity, structures and spectroscopy will be presented.
b) The third session will be dedicated to the study of complex systems and long range calculations;
c) And the fourth session will be dedicated to the study of solid state, molecule-surface interfaces and dynamical simulations.

New applications of the quantum chemistry methods on environmental problems and CO_2 storage will be evaluated.

Laptops are needed for practical exercises

We welcome all participants to Rabat.

Organizing Commitee

N. KOMIHA	Morocco (Rabat)	Chair of the conference
H. ABOU EL MAKARIM	Morocco (Rabat)	
K. MARAKCHI	Morocco (Rabat)	
O.K. KABBAJ	Morocco (Rabat)	
N. KOMIHA	Morocco (Rabat)	

Scientific Committee

H. ABOU EL MAKARIM	Morocco (Rabat)
D. BENOIT	United Kingdom (Hull)
D. BORGIS	France (Paris)
G. CHAMBAUD	France (Marne La Vallée)
F. X. COUDERT	France (Paris)
M. HOCHLAF	France (Marne La Vallée)
O. K. KABBAJ	Morocco (Rabat)
N. KOMIHA	Morocco (Rabat)
R. LINGUERRI	France (Marne La Vallée)
K. MARAKCHI	Morocco (Rabat)
M. L. SENENT	Spain (Madrid)

Table of contents

Articles

MOLECULAR MODELING OF OLIGOPEPTIDES CONTAINING CYSTEINE, GLYCINE AND ALANINE IN ISOLATED STATE

M. Bourjila[1,*], R. Tijar[1], B .EL Merbouh[1], A. Elguerdaoui[1], R. Drissi El Bouzaidi[1,2], and A. El Gridani[1]

[1]Laboratoire de chimie physique, Faculté des Sciences, B.P. 8106, Université Ibn Zohr, 80000, Agadir, Maroc.
[2]Centre Régional des Métiers de L'Education et de la Formation (CRMEF), Souss Massa Daraa, Inezgane, Maroc.

*Corresponding author email: malika.bourjila@edu.uiz.ac.ma

Abstract: The genetic algorithm based on the Multi-Niche Crowding (MNC) method is used with the semi-empirical method AM1 in order to scan the potential energy surface (PES) of peptides CysAla (AC), CysAla$_2$(CA$_2$), AlaCys (AC), Ala$_2$Cys (A$_2$C), GlyCys(GC), Gly$_2$Cys (G$_2$C), CysGly (CG) and CysGly$_2$(CG$_2$). The algorithm, implemented as a package of programs interfaced with MOPAC and piloted by scripts, provides better detection of local and global minima within a reasonable time. The Gas phase acidities of these peptides are also determined.

Keywords: MNC algorithm, AM1, peptides, Cysteine, Alanine, Glycine, PES.

INTRODUCTION

The conformational analysis of a molecular PES in the gas phase, allows the determination of the equilibrium structure. In this context, several methods of quantum computation have been developed especially ab initio ones. However, the use of these methods becomes very expensive in terms of time and resources especially for large molecular systems. AM1 is a semi-empirical method which has shown its reliability in theoretical treatment of conformational problems and can be used to approximate the equilibrium structure of a molecular system. In addition, in a multidimensional conformational space, the multiplicity of dihedral angles, the presence of heteroatoms and other factors, affect the convergence to equilibrium structures. Therefore, the determination of the global minima becomes increasingly complex. The genetic algorithm MNC program, coded by B. El Merbouh et al. [1], is characterized by an adequate system of conformational calculation providing a wide exploration and exploitation of space research studied in an acceptable time even for large molecular systems, mainly oligopeptides which are subject of this work.

As part of this work we are interested in studying the gas-phase acidity of peptides CysAla (AC), CysAla$_2$(CA$_2$), AlaCys (AC), Ala$_2$Cys (A$_2$C), GlyCys(GC), Gly$_2$Cys (G$_2$C), CysGly (CG) and CysGly$_2$(CG$_2$). We discuss their potential energy surfaces and analyze the main intrinsic factors that stabilize their equilibrium structures in the gas phase.

COMPUTATIONAL METHOD

The molecular potential energy surface PES was explored automatically by the multi-niche crowding genetic algorithm (MNC GA) coded by B. El Merbouh et al. [1]. The control parameters of this algorithm are given in Table 1. Individuals are represented by the

conformations and the genes by the dihedral angles. The heat of formation (function evolution) (evolution function) was calculated using semi-empirical method AM1. Through four steps namely selection, crossover, mutation and replacement using the worst among most similar WAMS technique (figure 1) [2], the global minimum and all local minima of each molecular PES are determined after several generations. The global minimum is the most stable conformation used to generate all structural and electronic proprieties of each molecular system.

The gas-phase acidity of a peptide whose deprotonation reaction is the following:

$$A H_{(g)} \longrightarrow A^-_{(g)} + H^+_{(g)}$$

is defined by the deprotonation enthalpy $\Delta_{acid}H$ deduced from the heat of formation of $HA_{(g)}$ and its conjugate base $A^-_{(g)}$ by the application of the following equation:

$\Delta_{acid}H = \Delta H°_f (A^-_{(g)}) + \Delta H°_f (H^+_{(g)}) - \Delta H°_f (AH_{(g)})$ with $\Delta H°_f (H^+_{(g)}) = 367.2$ kcal/mol.

Tableau 1. Control parameters of genetic algorithm program

|	
Population size	500
Crowding selection size (Cs)	25
Crowding Factor size (Cf)	3
Interval crossover parameter	10
Probability of crossover (Pc)	1.0
Probability of mutation (Pm)	0.06
Number of generation	100
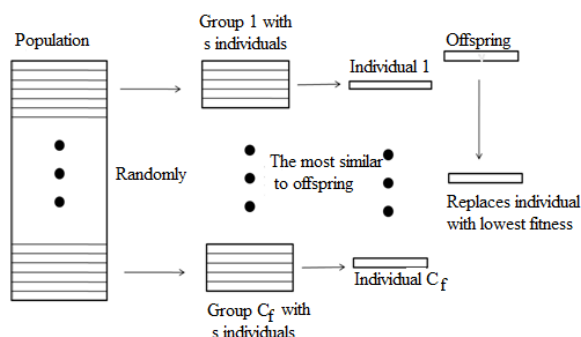
Figure1. Scheme of WAMS technique

RESULTS AND DISCUSSION

Equilibrium structures of peptides AC⁻, CA⁻, A₂C⁻, and CA₂⁻

The most stable conformers of AC⁻, CA⁻, A₂C⁻ and CA₂⁻, obtained by exploring the potential energy surfaces, are represented in figures 2,3,4 and 5 respectively. These equilibrium structures appear to be more stable than their counterparts obtained using other theoretical method [3]. Two factors may be evoked to justify this stability namely hydrogen bonds and steric effects.
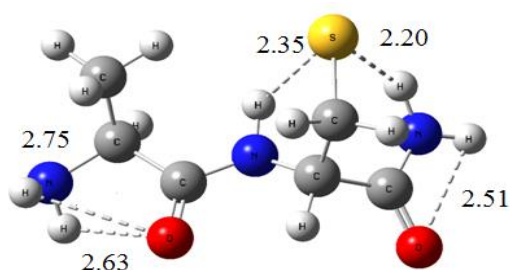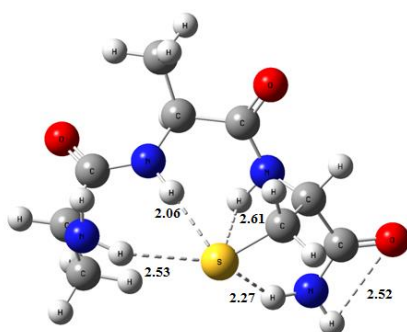

$\Delta H_f = -125.6$ kcal/mol

Figure 2. Most stable conformations of AC⁻ obtained using GA//AM1
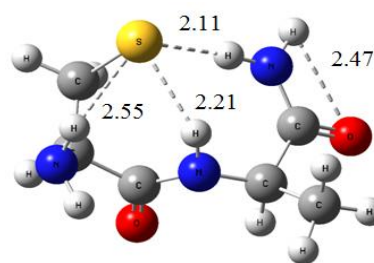
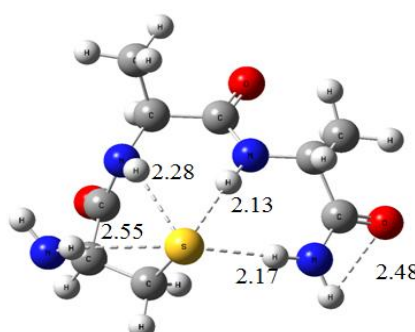$\Delta H_f = -130.6$ kcal/mol

Figure 3. Most stable conformation of CA⁻ obtained using GA//AM1

$\Delta H_f = -174.4$ kcal/mol

Figure 4. Most stable conformation of A_2C^- obtained using GA//AM1

$\Delta H_f = -180.1$ kcal/mol

Figure 5. Most stable conformation of CA_2^- obtained using GA//AM1

Gas phase acidities of (GC, CG, CG$_2$, G$_2$C, AC, CA, A$_2$C and CA$_2$)

Table 2 summarizes the gas phase acidities of the studied peptides. We notice that the acidity increases with the increase of the peptide chain which is in perfect agreement with the experimental results [3] and that it is largely determined by the structure of the anion $A^-_{(g)}$, where thiolate ion plays a key role.

Table 2. Gas phase acidities of peptides.

Peptide	Enthalpy for AH (kcal/mol)	Enthalpy for A$^-$ (kcal/mol)	Calculated $\Delta_{acid}H$(kcal/mol)	$\Delta_{acid}H$ (expt) [3] (kcal/mol)
GC	-86.0	-122.3	331.0	335.3
CG	-85.2	-127.8	324.6	330.4
G$_2$C	-123.2	-168.9	321.5	334.6
CG$_2$	-123.7	-173.7	317.2	329.7
AC	-89.7	-125.6	331.3	335.6
CA	-88.5	-130.6	325.1	331.2
A$_2$C	-130.1	-174.4	322.9	334.6
CA$_2$	-130.2	-180.1	317.3	330.5

CONCLUSION

The semi-empirical method AM1 shows that N-Cysteine are more acid than C-Cysteine as shown also experimentally.

Gas phase acidity increases with the increase of the peptide chain which is in perfect agreement with the experimental results. The equilibrium structures obtained in this study appear to be more stable than their counterparts obtained using other theoretical method which shows the performance of scanning of PES using a genetic algorithm.

The technique provides better detection of local and global minima within a reasonable time. It can be used to calculate the molecular PES of larger sizes peptides.

REFERENCES

[1] El Merbouh, B.; Bourjila, M.; Tijar, R.; Drissi El Bouzaidi, R.; El Gridani, A.; El Mouhtadi, M.; Conformational space analysis of neutral and protonated Glycine using a genetic algorithm for multi-modal search. Journal of Theoretical and Computational Chemistry, 13, **2014**, 1450067, 1-16.

[2] Cedenoa, W.; Rao Vemurib. V.; Analysis of speciation and niching in the multi-niche crowding GA. Theoretical Computer Science, 229, **1999**, 177-197.

[3] Shen. J.; Ren.J.;Gas phase acidity of a cysteine residue in small oligopeptides. International Journal of Mass Spectrometry, 316-318, **2012**, 147-156.

DFT & TD-DFT STUDIES OF THIAZOLOTHIAZOLE–BASED ORGANIC DYES FOR DSSCs

Asmae Fitri[1], Adil Touimi Benjelloun[1,*], Mohammed Benzakour[1], Mohammed Mcharfi[1], Mohammed Hamidi[2] and Mohammed Bouachrine[3]

[1]ECIM/LIMME, Faculty of Sciences Dhar El Mahraz, University Sidi Mohamed Ben Abdallah, Fez, Morocco
[2]URMM/UCTA, FST Errachidia, University Moulay Ismaïl, Errachidia, Morocco
[3]ESTM, (LASMAR), University Moulay Ismaïl, Meknes, Morocco

*Corresponding author email: tbadil@yahoo.com

Abstract: In this study, we have designed four novel organic donor–π–acceptor dyes (D1, D2, D3, D4), used for dye sensitized solar cells (DSSCs). These dyes, based on thiazolothiazole as π-spacer, were studied by density functional theory (DFT) and its extensible time dependent DFT (TDDFT) approaches to shed light on how the π–conjugation order influence the performance of the dyes in the DSSCs. The theoretical results have shown that the LUMO and HOMO energy levels of these dyes can ensure positive effect on the process of electron injection and dye regeneration. Key parameters in close connection with the short–circuit current density (Jsc), including light harvesting efficiency (LHE), injection driving force (ΔG^{inject}) and total reorganization energy (λ_{total}), were discussed. The calculated results reveal that dye D2 can be used as a potential sensitizer for TiO_2 nanocrystalline solar cells due to its best electronic and optical properties and good photovoltaic parameters.

Keywords: Dye sensitized solar cells; thiazolothiazole; TDDFT, PCM; optoelectronic; photovoltaic parameters

INTRODUCTION

DSSCs have attracted significant attention in scientific research and in practical applications due to their high efficiencies and low costs, since the first report by O'Regan and Grätzel in 1991 [1-3]. A typical DSSC based on organic dyes is constructed with a wide band gap semi–conductor (typically TiO_2) sensitized with molecular dyes, able to capture light in the visible region of the spectrum, electrolyte containing Iodide/triiodide (I^-/I_3^-) redox couple, and a platinum counter electrode [4-8]. In these cells, the sensitizers play an important role of capturing solar energy and generating electric charges. The most extensively studied organic dyes usually adopt the donor–π spacer–acceptor (D-π-A) structural motif in order to improve the efficiency of the UV/Visible (UV/Vis) photoinducted intramolecular charge transfer (ICT) [9]. In this structure, the ICT from D to A at the photoexcitation will inject the photoelectron into the conduction band of the semiconductor through the electron accepting group at the anchoring unit.

As we know, thiazolothiazole is rigid, coplanar and electron–accepting fused heterocycle due to the electron–withdrawing nitrogen of imine (C=N) and giving rise to a highly extended π-electron system [10]. Considering lots of advantages of the thiazolothiazole as π-spacer

together the most commonly used cyanoacrylic acid acceptor, and the excellent electron donating ability of coumarin, indoline, carbazole and triphenylamine, we decided in this work to design new four organic D1, D2, D3 and D4 thiazolothiazole-based dyes (Figure 1(a)).
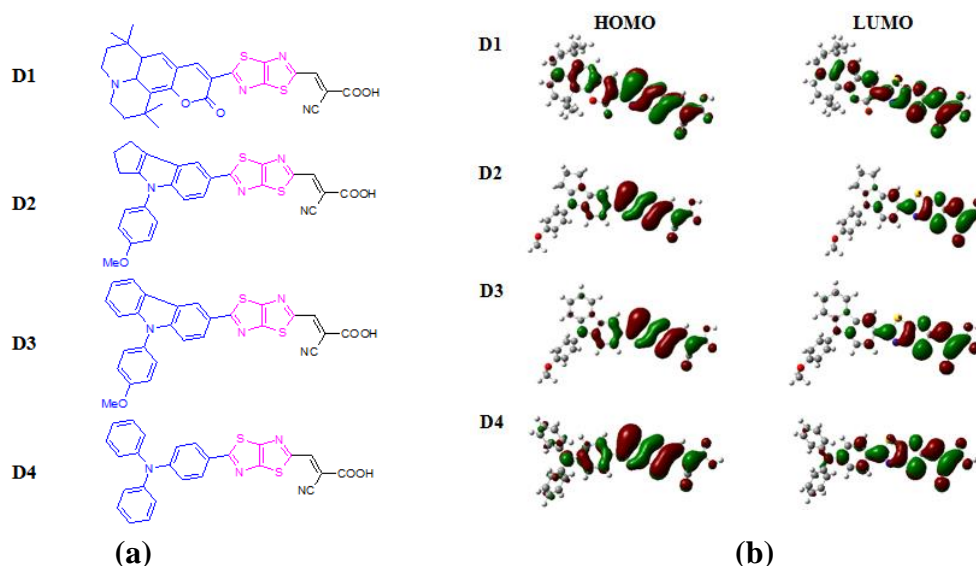

Figure 1. Molecular structure of studied dyes (a) and their frontier HOMO and LUMO orbitals (b) optimized with DFT at the B3LYP/6–31+G (d, p) level.

MATERIALS AND METHODS

All the calculations were performed with the Gaussian 09 packages [11]. The ground-state geometries were optimized using density functional theory (DFT) with B3LYP/6-31 G (d, p) basis set [12–14]. The UV-vis spectra were obtained by TDDFT calculations with CAM-B3LYP [15] functional with solvation effects included (chloroform). The cationic and anionic states were optimized at the B3LYP/6–31+G (d, p) level to calculate the total reorganization energies (λ_{total}).

RESULTS AND DISCUSSION

Figure 1(b) shows the optimized molecular structure and frontier molecular orbitals of studied dyes. As observed, the electron distributions of HOMOs are mainly localized on the electron donor groups and conjugated spacer, whereas the electron distribution of LUMOs are mainly localized on the π-spacer and acceptor units (mostly on the anchoring group), which indicates that there are good electron-separated states between HOMOs and LUMOs. Therefore, we could expect that there would be intramolecular charge transfer when the transition occurs, which is beneficial for the photoexcitation electrons injection. The anchoring group (–COOH) of all dyes has considerable contribution to the LUMOs which could lead to a strong electronic coupling with TiO$_2$ surface and thus improve the electron injection efficiency.

As expected in Figure 2, the HOMO energies of all dyes are lower than that of I^-/I_3^- (*ca.* -4.8 eV) [16], therefore, these molecules that lose electrons could be restored by getting electrons from electrolyte. Simultaneously, the LUMO energy levels of all dyes are much higher than that of TiO$_2$ conduction band edge (*ca.* –4.0 eV) [17], which is responsible for an effective injection of excited electrons. Thus, electron injection of excited molecules and,

subsequently, regeneration of the oxidized species is energetically permitted. This allows the application of the studied dyes in DSSC.

The simulated absorption spectra are shown in Figure 3. The spectra show similar profile for all dyes which present a main intense band at higher energies from 433 to 472 nm, and are assigned to the ICT transitions. For the four dyes, the strongest absorption peaks arise from the ground state (S_0) to the first excited state (S_1), which corresponds to the dominant promotion of an electron from HOMO to LUMO.
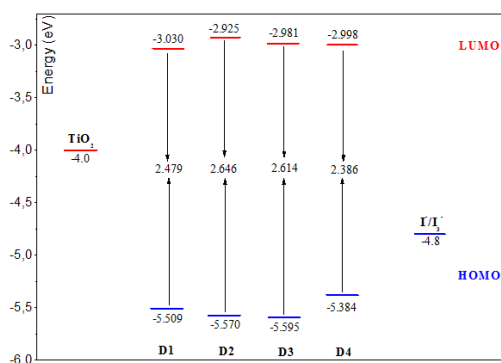

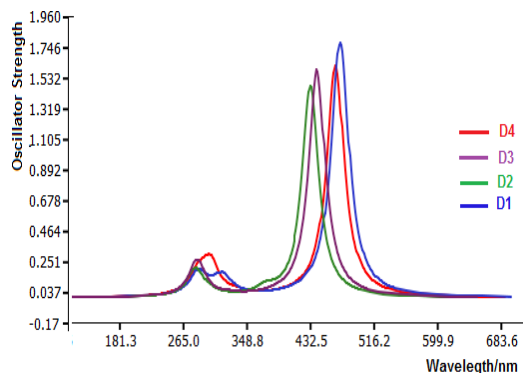**Figure 2.** Schematic energy diagram of all dyes, TiO₂ and electrolyte (I^-/I_3^-).

Figure 3. Simulated absorption spectra of all dyes in chloroform.

The injection driving force (ΔG^{inject}), light harvesting efficiency (LHE), and total reorganization energy (λ_{total}) have been investigated to see the sensitizer donor effects on the short-circuit current density (Jsc); the results are regrouped in Table 1.

Table 1. Estimated electrochemical parameters for all dyes.

Dye	ΔG^{inject} (eV)	LHE	λ_h (eV)	λ_e (eV)	λ_{total} (eV)
D1	-1.12	0.98	0.23	0.38	0.61
D2	-1.29	0.97	0.20	0.34	0.54
D3	-1.22	0.97	0.19	0.34	0.53
D4	-1.28	0.98	0.12	0.44	0.56

As showing in Table 1, the LHE values for these dyes are in narrow range (0.97 - 0.98). This means that all the sensitizers give similar photocurrent. In addition, these dyes have negative ΔG^{inject}, implying that the electron injection process is spontaneous, and the calculated ΔG^{inject} is decreased in the order of D2 > D4 > D3 > D1. On the other hand, the calculated λ_{total} shows that D3 and D2 possess the smallest total reorganization energy while D4 and D1 have the largest. Furthermore, it distinctly shows that the differences between λ_h and λ_e of the designed dyes are 0.15, 0.14, 0.15 and 0.32 eV, respectively. Thus, the differences of D2 result in a more balanced transport rates than other dyes.

CONCLUSION

As a result, (combing with the discussion of) after comparing the electron injection driving force, light harvesting efficiency, and the reorganization energies of the studied organic dyes, we could predict that dye D2 exhibits a favorable *Jsc* than other dyes.

REFERENCES

[1] O'Regan, B; Grätzel, M. A low-cost, high-efficiency solar cell based on dye-sensitized colloidal TiO$_2$ films, *Nature* **1991**, *353*, 737-740.

[2] Hagfeldt, A.; Grätzel, M. Molecular Photovoltaics *Acc. Chem. Res.* **2000**, *33*, 269-277.

[3] Grätzel, M. Photoelectrochemical cells, *Nature* **2001**, *414*, 338-344.

[4] Heimer, T.A.; Heilweil, E.J.; Bignozzi, C.A.; Meyer G. Electron Injection Recombination and Halide Oxidation Dynamics at Dye-sensitized TiO$_2$ Interfaces, *J. Phys. Chem. A* **2000**, *104*, 4256-4262.

[5] Nazeeruddin, M.K. Dye sensitized solar cells: Michael Grätzel Festschrift, a tribute for his 60th birthday: special issue. *Coord. Chem. Rev.* **2004**, *248*, 1161-1164.

[6] Kamat, P.V.; Haria, M.; Hotchandani, S. C60 Cluster as an Electron Shuttle in a Ru(II)-Polypyridyl Sensitizer Based Photochemical Solar Cell. *J. Phys. Chem. B* **2004**, *108*, 5166-5170.

[7] Bisquert, J.; Cahen, D.; Hodes, G.; Ruehle, S.; Zaban, A. Physical Chemical Principles of Photovoltaic Conversion with Nano- particulate, Mesoporous Dye-Sensitized Solar Cells. *J. Phys. Chem. B* **2004**, *108*, 8106-8118.

[8] Furube, A.; Katoh, R.; Yoshihara, T.; Hara, K.; Murata, S.; Arakawa, H. Ultrafast Direct and Indirect Electron-Injection Processes in a Photoexcited Dye-Sensitized Nanocrystalline Zinc Oxide Film: The Importance of Exciplex Intermediates at the Surface. *J. Phys. Chem. B* **2004**, *108*, 12583-12592.

[9] Preat, J.; Jacquemin, D.; Michaux, C; Perpète, E.A. Improvement of the efficiency of thiophene bridged compounds for dye-sensitized solar cells. *Chem. Phys.,* **2010**, *376*, 56-68.

[10] a)Fitri, A.; Touimi Benjelloun, A.; Benzakour, M.; Mcharfi, M.; Sfaira, M.; Hamidi, M.; *et al.* New materials based on thiazolothiazole and thiophene candidates for optoelectronic device applications: theoretical investigations. *Res Chem Interm.* **2013,** *39*, 2679-2695.b) Fitri, A.; Touimi Benjelloun, A.; Benzakour, M.; Mcharfi, M.; Hamidi, M.; Bouachrine, M. Theoretical investigation of new thiazolothiazole-based D-p-A organic dyes for efficient Dye-Sensitized Solar Cell. *Spectrochim. Acta A: Mol. Biomol. Spectrosc*. **2014**, *124,* 646-654.

[11] Frisch, M.J.; Trucks, G.W.; Schlegel, H.B.; Scuseria, GE; Robb, M.A.; Cheeseman, J.R.; et al. Gaussian 09, revision A.02. Pittsburgh PA: Gaussian, Inc; **2009**.

[12] Becke, A.D. A new mixing of Hartree–Fock and local density functional theories. *J. Chem. Phys.* **1993**, *98*, 1372-1377.

[13] Becke, A.D. A new mixing of Hartree-Fock and local density functional in atoms, molecules, and solids by the spin-density-functional formalism. *Phys. Rev. A* **1988**; *38*, 3098-3100.

[14] Lee, C.; Yang, W.; Parr, R.G. Development of the Colle-Salvetti conelation energy formula into a functional of the electron density. *Rev. B* **1988**, *37*, 785-789.

[15] Yanai, T; Tew, D.P.; Handy, N.C. A new hybrid exchange–correlation functional using the Coulomb-attenuating method (CAM-B3LYP). *Chem. Phys. Lett.* **2004**, *393*, 51-57.

[16] Hagfeldt, A.; Grätzel, M. Light-Induced Redox Reactions in Nanocrystalline Systems. *Chem. Rev.* **1995**, *95*, 49-68.

[17] Asbury, J.B.; Wang, Y.Q.; Hao, E; Ghosh, H; Lian, T. Evidences of hot excited state electron injection from sensitizer molecules to TiO_2 nanocrystalline thin films. *Res. Chem. Intermed.* **2001**, *27*, 393-406.

QUANTUM STUDY OF THE INTERACTION OF MERCURY ATOM WITH THE ATMOSPHERIC RADICAL SH

N. Ezarfi, A. Touimi Benjelloun[*], S. Sabor, M. Benzakour, M. Mcharfi and A. Daoudi

Equipe de Chimie Informatique et Modélisation (ECIM). Laboratoire d'Ingénierie des Matériaux, de Modélisation et d'Environnement (LIMME), University Sidi Mohammed Ben Abdallah (USMBA), Faculty of Sciences Dhar El Mahraz, Department of chemistry, BP. 1796, Fez - Morocco.

*Corresponding author email: tbadil@yahoo.com

Abstract: The ground state potential hyper surface $^2A'$ has been studied through density functional theory (DFT) methods for the Hg(SH) complex. Two processes have been identified. The first one concerns the hydrogen inversion process in the coordination of HgSH and the second one is about the isomerization of HgSH into HHgS. Four stationary points have been found; two of them correspond to the stable structures with symmetries: HgSH($^2A'$), HHgS($^2\Pi$), and two correspond to transition states [TS] with the symmetries HgSH($^2\Sigma^+$), HgSH($^2A'$). The energetic, structural, spectroscopy, and thermodynamics results obtained at various levels through, e.g., DFT with B3LYP exchange-correlation functionals and CCSD(T) are presented for the whole set of the stationary points and their dissociation products. Reactions of mercury (Hg) with atmospheric molecules (SH, HS_2, and S_2) have been studied at various levels of approximation in order to study the possible existence of HgSH in the atmosphere.

Keywords: Mercury, radical SH, DFT, ab initio, hypersurface, spectroscopic properties.

INTRODUCTION

Mercury (Hg) is known to be one of the most scattered heavy metals into the atmosphere. Its toxic action on living organisms has been proven, it interferes with various enzymatic systems through links to OH , SH, NO... active sites, or through displacement of other metals essential to the organism, such as Fe, Ca, Pb, Hg, Zn, ... leading to Alzheimer's disease, chronic fatigue syndrome, fibromyalgia and other chronic diseases. Once emitted into the atmospheric medium, Hg in particle or gaze phase meets radicals or molecules in the different levels of atmosphere, where chemical reaction can occur, perturbing accordingly the chemical equilibrium of this medium. In this work, we are interested on the study of the interaction of Hg with SH leading to the Hg(SH) species in its two forms HHgS and HHgS.

MATERIALS AND METHODS

Two methodologies have been used in this work in order to take into account the correlation effects, which are known to be important for heavy atoms, namely, the ab initio with the coupled cluster CCSD(T) [1] method following an unrestricted Hartree-Fock (UHF) [2] calculation, and the density functional theory (DFT) in its standard unrestricted Kohn-Sham

formalism [3]. In the DFT methodology, a variety of exchange-correlation functionals have been proposed during these last two decades, and the most widely used are available in spread computational codes such as GAUSSIAN 03 (G03).

BASIS SETS

For our study in the context of these two methodologies, we used the G03 code (Gaussian03), choosing a variety of atomic basis functions using Gaussian-type (GTO). For atmospheric species, we adopted two basis sets, one for the correlation consistent Dunning polarized triple zeta quality for the valence orbitals and augmented by diffuse functions denoted aug-cc-pVTZ contracted:

6s3p2d) s(3,1,1,1)p(1,1,1)d(1,1) for H.

(17s6p3d2f) s(7,7,1,1,1)p(3,1,1,1)d(1,1,1)f(1,1) for O.

For heavy metals (Mercury), the treatment requires special atomic orbital basis that are introduced including relativistic effects.
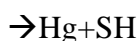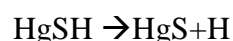
- MWB60 (quasi relativistic) de Wood Boring [4]:
  (8s, 7p, 6d)-[s(3,1,1,1,1,1),p(2,2,1,1,1),d(4,1,1)

- cc-pwCVTZ-PP [5] with 60 electrons frozen:
  (16s, 20p, 12d, 2f)-[s(7,7,1,1),p(6,6,6,1,1),d(5,5,1,1),f(1,1)]

RESULTS AND DISCUSSION

To our knowledge, HgSH and HHgS molecules have never been studied (neither) experimentally but in literature, some works provide HgSH radical bent state [6]. The two following association and isomerization reactions have accordingly been studied:

$$Hg + SH \rightarrow HgSH$$

$$HgSH \rightarrow HHgS$$

as well as the dissociation products of both isomers:

$$HgSH \rightarrow HgS+H \qquad HHgS \rightarrow HgH+S$$

$$\rightarrow Hg+SH \qquad \rightarrow HgS+H$$

Several approaches are possible to generate the Hg(SH) system. The interaction of Hg with SH occurred in different symmetries: collinear $C_{\infty v}$ or bent Cs. Different paths to form the complex Hg(SH):

$$Hg\ (^1S) + SH\ (^2\Pi) \rightarrow Hg\ (SH)\ (^2\Pi, {}^2A")$$

$$HgH(^2\Sigma^+) + S(^3P) \rightarrow Hg(SH)\ ({}^{2,4}\Sigma^+, {}^{2,4}\Pi, {}^{2,4}A', {}^{2,4}A")$$

$$HgS(^1\Sigma^+) + H(^2S) \rightarrow Hg(SH)\ ({}^2\Sigma^+, {}^2A')$$

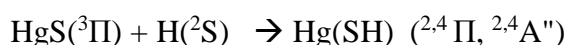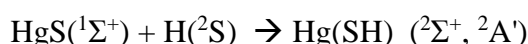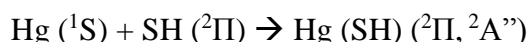$$HgS(^3\Pi) + H(^2S) \rightarrow Hg(SH)\ ({}^{2,4}\Pi, {}^{2,4}A")$$

Table 1. Thermal dissociation energies and the existence domain of isomers HgSH and SHgH calculated at B3LYP.

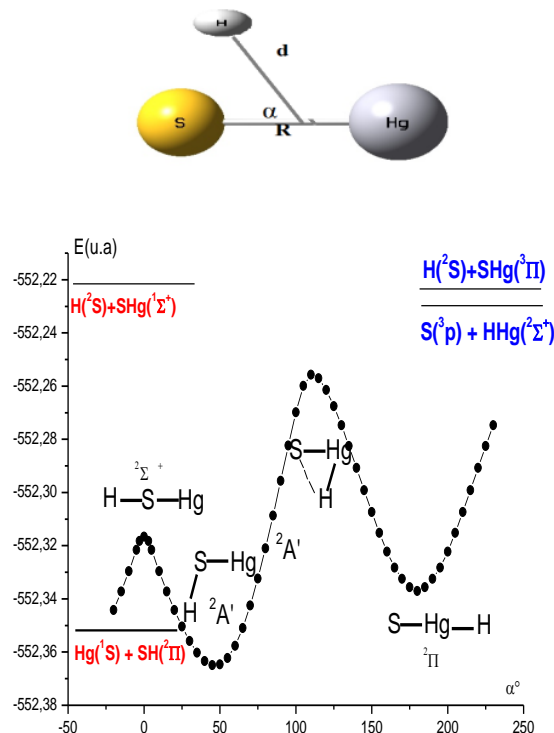|	$\Delta H_{298}°$ (Kcal/mol)	λ(nm)	domain
HgSH → HgS+H	87.16	328.0	UV
HgSH → Hg+ SH	8.36	3419.9	IR
HHgS → HgH+S	63.88	447.6	visible
HHgS → HgS+H	66.21	431.8	visible

Figure 1. Ground potential energy curves of the HgSH→HHgS isomerization process calculated at, B3LYP. The abscissa is the α spheroid angle as illustrated in the upper of the top panel; points on the curves are energies minimized with respect to variables *d* and *R*. The energy levels of possible dissociation limits are also indicated.

1. Analyzing the potential hyper surface ^{2}A' of Hg(SH) complex reveals :
-Two processes have been identified. The first one concerns the hydrogen inversion process in the coordination of HgSH and the second one is the isomerization of HgSH into HHgS.
-Four stationary points have been found; two of them correspond to the stable structures with symmetries HgSH(^{2}A'), HHgS ($^2\Pi$) and the other two correspond to transition states [TS] with the symmetries HgSH($^2\Sigma^+$), HgSH(^{2}A').

2. Stability of the Hg(SH) complex in the atmosphere:
-The formation of isomers HgSH and HHgS by reaction of mercury atom with hydrosulfide radical SH is possible;
-The bent HgSH forms (with a valence angle of 91.6 °) are more stable than the linear isomer HHgS;
-Transition states are found below the dissociation limits and providing the isomerization process is easy.
-We expect that HgSH isomer (^{2}A') can photodissociate in the presence of sunlight, and regenerate overnight.

CONCLUSION

Examination of the stability of the complex Hg(SH) by the DFT method (B3LYP/MWB60) shows that the bent HgSH form is the most stable, but the existence in the atmosphere of the SHgH isomer is more favorable with $\Delta H°_{298} = 65$ kcal/mol. Also we note that the complex Hg(SH) is easily dissociated in the presence of the solar radius during the day and accumulates during the night by exothermic reactions.

REFERENCES

[1] Pople, J. A.; Head-Gordon M.; Raghavachari, K. Fifth order Moeller-Plesset perturbation theory: comparison of existing correlation methods and implementation of new methods correct to fifth order *J. Chem. Phys.* **1987,** *87*, 5968.

[2] Pople, J. A.; Nesbet, R. K.; Berthier, G. *J. Chem. Phys*. **1954**, *22*, 571.

[3] Kohn, W. and Sham, L. Density-functional approximation for the correlation energy of the inhomogeneous electron gas *Phys. Rev. B* **1986**, *33*, 8800.

[4] Tossel, J. A. *J. Phys. Chem.* A **2001**, 105, 935.

[5] Andrae, D.; Haeussermann, U.; Dolg, M.; Stoll, H.; Preuss, H. Energy-adjustedab initio pseudopotentials for the second and third row transition elements. *Theor. Chim. Acta* **1990,** *77*, 123.

[6] Dieter, K.; ELFI, K.; Michael, F.; Bonding in mercury molecules described by the normalized elimination of the small component and coupled cluster theory, *Chem. Phys. Chem.* **2008**, *9*, 2510-2521.

π STACKING INTERACTION INVOLVING A EXCITED STATE: TOWARDS A FORCE FIELD REPRESENTATION

Karim Merabti[1,2,*], Sihem Azizi[1], Isabelle Demachy[2], Bernard Lévy[2]

and Jacqueline Ridard[2]

[1]Laboratoire de Physique Théorique, Université Abou Bekr Belkaid, Tlemcen, Algérie
[2]Laboratoire de Chimie Physique d'Orsay, Université de Paris-Sud, 91405 Orsay Cedex, France

*Corresponding author email: hadj.merabti@gmail.com

Abstract: The π staking interaction is significantly different in the ground state and the excited state. Hence we need to modify the corresponding van der Waals parameter in the force field to be used in molecular dynamics. We evaluated the interaction energy between the chromophore and the tyrosine in the excited state with ab initio method quantum chemistry CASPT2. We intend to use the resulting force fields in the study of Yellow fluorescent Protein (YFP).

INTRODUCTION

Fluorescent proteins are naturally occurring substances in the jellyfish, corals, sea anemones and a few others [1,2]. They are used in the laboratory as probes capable of measuring the local pH, the temperature and the distance between proteins. They are also one of the possible carriers of ultra-microscopy [3]. The theoretical approaches combine methods of molecular dynamics and quantum chemistry to find new fluorescent proteins and understand the dynamics of the protein environment. This work present a theoretical study of π-stacking interaction between the chromophore and a tyrosine in YFP (yellow fluorescent protein) [4], where the electronic transition energy is reduced compared to that of Green fluorescent Protein (GFP) due to the influence of the π stacking between the Chromophore and that Tyrosine. This type of interaction is poorly described in exited states by usual force fields. Our objective is to determine a specific force field to describe the effect of π stacking interactions on the dynamics of the excited chromophore in YFP and on the fluorescence properties.
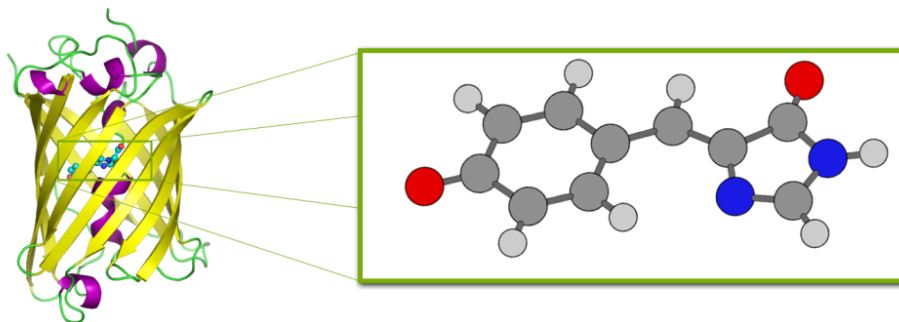

Figure 1. Left a fluorescent protein and right the chromophore (anionic form)

RESULTS AND DISCUSSION

- The xy axes of the system (Figure 2) are defined in the atoms of the chromophore and the z axis is perpendicular to the xy plane.
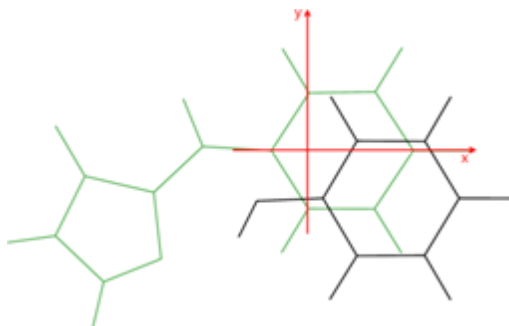

Figure 2. Geometry of the complex (Cro-Tyr) for x = 1 Å, y = -1 Å

Tyrosine is moved in the xy plane with a pitch of 0.5 Å and for different distances z between the two rounds of 2.5 to 4 Å, for all the movements of the Tyrosine we calculate the interaction energy.

Then, we interpolate the energy values to adjust the parameters of the force field to make a new molecular dynamics with force fields. Tyrosine is moved in the xy plane with a pitch of 0.5Å and for different distances z between the two rounds of 2.5 to 4Å, for all the movements of the Tyrosine we calculate the interaction energy. The interaction energy is calculated between two molecules (Chromophore and Tyrosine) with BSSE (Basis Set Superposition Error) 5 corrections by the approach of Counterpoise CP:

$$\Delta E = E \ (cro+tyr) - E^{cp}(cro) - E^{cp}(tyr)$$

We calculated the energy with the 6-31G* basis set, by the CASPT2 [6,7] method (complete active space second-order perturbation theory).CASSCF calculations in a minimal active space (4 electrons and 3 orbitals) with geometry optimization in the state averaged approach SA2-CAS [4,3] were performed. This level of theory is compatible with a large number of calculations of energy [8]:
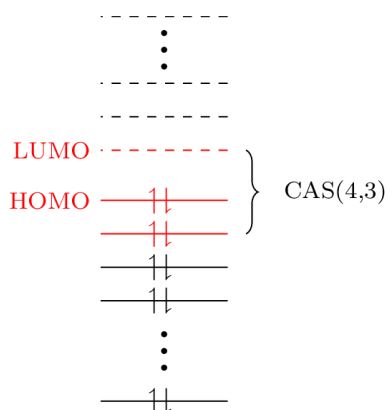
In the CASPT2 calculations, we have to consider carefully the number of active orbitals in the complex formed by the chromophore and the tyrosine. The active space has to be balanced regarding the ones of the separate systems.

Looking for intruder states: TDDFT calculations using localised orbitals provide evidence that both local excitations and electron transfer are present in the same energy range.
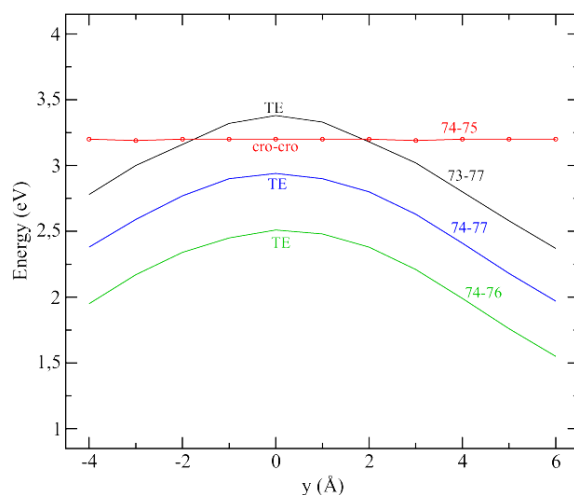
Figure 3. Energy transitions as a function of y with x = 1 Å and z = 3.5 Å

However, we remark a crossing (74-75, 73-77) and the energy difference between the charge transfer and intermolecular excitation is large.

CONCLUSION

The pi-stacking may result in degeneracy between the local excited state and charge transfer; we need to define a minimal active space representing the degeneracy and as perspective, we will interpolated the energy values to adjust the parameters of the force field to make a new molecular dynamics with force fields.

REFERENCES

[1] Tsien, R. Y. THE GREEN FLUORESCENT PROTEIN. Annual Review of Biochemistry **1998**, 67 (1), 509-544.

[2] Wachter, R. M. The Family of GFP-Like Proteins: Structure, Function, Photophysics and Biosensor Applications. Photochemistry and Photobiology **2006**, 82 (2), 339-344.

[3] Nienhaus, K.; Ulrich Nienhaus, G. Fluorescent proteins for live-cell imaging with super-resolution. Chem. Soc. Rev., The Royal Society of Chemistry **2014**, 43, 1088-1106.

[4] Wachter, R. M. E. M.-A. . K. K. H. G. T. &. R. S. J. Structural basis of spectral shifts in the yellow-emission variants of green fluorescent protein. Structure **1998**, 6,1267-1277.

[5] Boys, S. &. B. F. The calculation of small molecular interactions by the differences of separate total energies. Some procedures with reduced errors. Molecular Physics **1970**, 19 (4), 553-566.

[6] Werner, H.-J. Mol. Phys **1996**, 89, 645-661.

[7] P. Celani and H.-J. Werner, J. Chem. Phys **2000**, 112, 5546.

[8] Jonasson, G.; Teuler, J.-m.; Vallverdu, G.; Merola, F.; Ridard, J.; Levy, B.; Demachy, I. Excited State Dynamics of the Green Fluorescent Protein on the Nanosecond Time Scale. Journal of Chemical Theory and Computation **2011**, 7, 1990-1997.

AB-INITIO STUDY OF 2D FULLY HYDROGENATED SIC HONEYCOMB CONFORMERS

L. B. Drissi*, K. Sadki, F. El yahyaoui and E. H Saidi

LPHE, Modeling and Simulations, Faculty of Science, Mohammed V University, Rabat, Morocco

*Corresponding author email: drissilb@gmail.com

Abstract: By using ab initio calculations based on density-functional theory, we study the structural and electronic properties of pristine and five possible conformers of fully hydrogenated SiC honeycomb sheet. In particular, we study the stability of these structures based on the forming and binding energy, and we investigate their electronic properties based on the band structures and density of states (DOS). Our results reveal that apart table conformer, all the other configurations, namely chair, zigzag, boat and armchair are dynamically stable and are also semiconductors with direct band gaps much larger than 2.5 eV of pristine SiC sheet.

Keywords: Silicene; Graphene; Hydrogenation; Ab-initio calculations; DOS; Band structure.

INTRODUCTION

Since its successful synthesis, graphene [1,2] has been the subject of intensive studies because of its various important properties, such as high mobility and ballistic transport over long distances, very required for making high-quality electronic devices.

The rapid rise of graphene research has simulated a lot of work to investigate the honeycomb lattices of other group IV elements, such as silicon that has also four valence electrons like carbon [3]. Among the group IV elements, only carbon can take either sp^2 or sp^3 bond configuration and form 2D layered structure. Silicon prefers sp^3 instead of sp^2 hybridization. However, it is possible to form layered structure by mixing C and Si [4].

Chemical modifications, especially the hydrogenation [5] and the fluorination [6] in 2D honeycomb systems, have enhanced foreseen applications in nanotechnology. In particular, the chemical modification with H is a promising way to create a band gap in 2D semi-metals as graphene and silicone [7, 8].

Recently, a 2D hydrocarbon material in the family of honeycomb structure, namely SiC was synthesized [9]. The pristine SiC conformers are revealed to be a semi-metal with an energy gap of 2.5eV.

In this paper, the structural and electronic properties of the pristine and all possible conformers of fully hydrogenated SiC sheet are presented. Using the density functional theory, we calculated the binding energy, the formation energy and the band gap for the different conformers. It results that, except table conformer, all the other configurations are dynamically stable, with binding energy ranging from -1.967 to -1.942 eV and are also semiconductors with direct band gaps.

RESULTS AND DISCUSSION

Hexagonal SiC hybrid is a 2-dimensional planar sheet, with Si and C atoms occupying the A and B sublattices of a 2D honeycomb plane as showed in FIG. 1- a and b. In what follows, we study the effect of hydrogen atoms positions on different conformers of full-hydrogenated SiC sheet. As showed in Figure 2, chemical modification with H atoms leads to five possible configurations, namely chair, zigzag, boat, armchair and table.
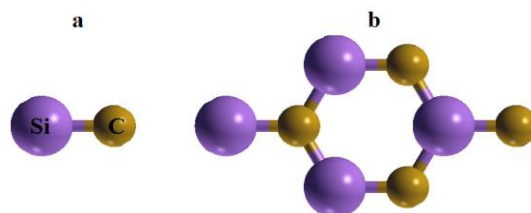

Figure 1. a) The unitcell of SiC sheet, violet (brown) color correspond to Si (C) sites, b) the (2×2) supercell of SiC hybrid.

The optimized geometric structures of pristine SiC and full-hydrogenated SiC, namely chair, zigzag, boat, armchair and table conformers lead to the following data: in the chair conformer where the hydrogen atoms are alternatively attached to the Si/C atoms on both sides of the plane, we find that SiC bond d(Si-C) = 1.895Å. In the zigzag conformer where three consecutive hydrogen atoms of each hexagon are alternatively attached to the Si/C atoms on both sides of the sheet, the distances between the atoms are d_1(Si-C)= 1.884Å and d_2(Si-C) = 1.90Å. In the boat conformer where the hydrogen atoms are alternatively attached in pairs to the Si/C atoms on both sides, the calculations of geometric structure give d_1(Si-C) = 1.886Å and d_2(Si-C) = 1.91Å. In the armchair conformer where all the hydrogen atoms are attached to the Si/C atoms involving armchair direction in upside and the other in down side, d_1(Si-C) =1.887Å , d_2(Si-C) =1.895Å and d_3(Si-C) = 1.91Å. In the table conformer where the hydrogen atoms are attached to the Si/C atoms from only one side, the bond length is d(Si-C) = 1.908Å. We deduce that the Si-C bond lengths of all the conformers are larger than the one in pristine SiC sheet. Moreover, the buckling of all the conformers are ranging from a minimal value of 0.23Å to a maximal value of 1.39Å corresponding to the table and armchair conformer, respectively.

(a) chair   (b) zigzag   (c) boat   (d) armchair   (e) table
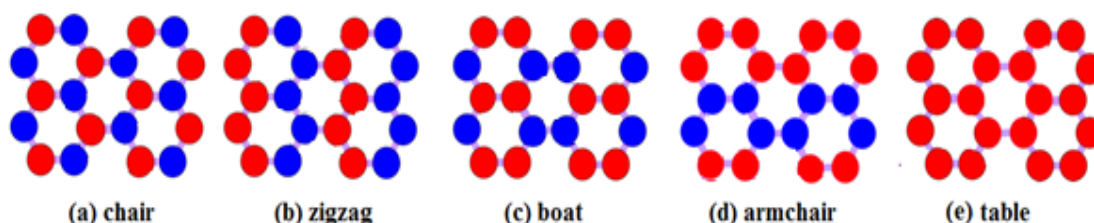
Figure 2. The Five hydrogenated conformers of silicane-graphane: a) chair, b) zigzag, c) boat, d) armchair and (e) table conformers. The red/blue colors represent adsorbates H above/below the SiC sheet.

To evaluate the structural stability of fully hydrogenated SiC, we calculate the associated formation and binding energy. The formation energies are -0.280, -0.270, -0.261, -0.255 and 0.072 eV per atom, for the chair, boat, zigzag, armchair and table conformer respectively. However, all the binding energy have negative values -1.967, -1.957,-1.948, -1.942

and -1.615 eV/atom for the chair, boat, zigzag, armchair and table conformer respectively. This result indicates that with the exception of table conformer, all the other conformers are thermodynamically stable. Moreover, like graphane [10] and silicane [8], chair configuration is the most stable one for hydrogenated SiC hybrids.

To investigate the electronic properties of these new hybrids, we run ab-initio calculations using the generalized gradient approximation (GGA) of Perdew, Burke, and Ernzerhof (PBE). From Figure 3 we show that upon hydrogenation, the electronic band structure of the five hydrogenated conformers produces remarkable changes compared to the pristine SiC sheet that is semi-conductor with a band gap of 2.53eV [4]. Indeed, the electronic structure of both the chair and zigzag conformers shows a large direct band gap (at the Γ point) of 4.04 and 3.84 eV while the table, boat, and armchair have an indirect band gap with the values of 3.55, 4.21 and 4.39 eV, respectively.
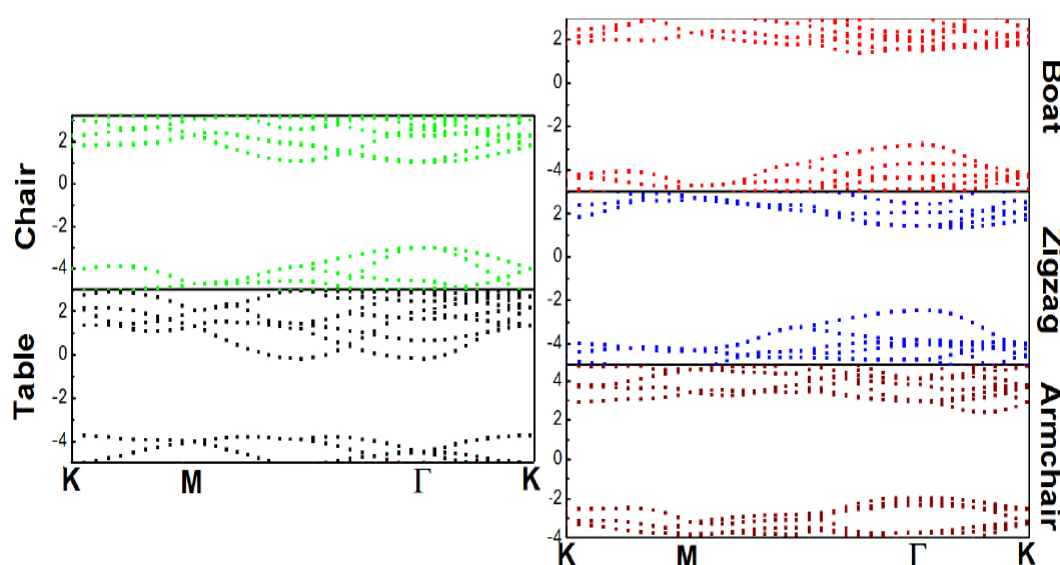
Figure 3. Band structures corresponding to the five hydrogenated SiC hybrids conformers plotted in the two dimensional Brillouin zone.

CONCLUSION

In conclusion, the structural stability and electronic properties of chair, zigzag, boat, table and armchair full hydrogenated SiC sheets were investigated based on the ab initio calculations according to the density-functional theory. The calculations reveal that all these structures are dynamically stable, except table conformer that shows positive formation energy. As their counterpart pristine SiC sheet, the five configurations are semiconductors with direct large band gaps.

In general, surface modification with H atoms can significantly change the fundamental properties of the SiC sheet, which shows a promising potential application in new generation of nano-electronics and spintronics materials.

MATERIALS AND METHODS

We use the Quantum espresso (QE) simulation package and the density functional theory (DFT) within generalized gradient approximation (GGA) and the exchange-correlation potential. The ultra-soft pseudo-potential (USPP) is employed to describe the electron–electron interactions. The Monkhorst-Pack k-point grid size of 8×8×1 and 16×16×1 were used for structural properties and for electronic properties calculations respectively.

The energy convergence is smaller than 10^{-4} eV. A maximum force of 0.002 eV/Å was allowed on each atom.

REFERENCES

[1] Geim, A. K.; Novoselov, K. S. The rise of graphene. Nature Materials. **2007**, 6, 183-191.

[2] Drissi, L. B.; Saidi, E. H.; Bousmina, M. Four-dimensional graphene. Phys. Rev. D. **2011**, 84, 014504.

[3] Takeda, K.; Shiraishi, K. Theoretical possibility of stage corrugation in Si and Ge analogs of graphite. Phys. Rev. B. **1994**, 50, 14916.

[4] Drissi, L. B.; Saidi, E. H.; Bousmina, M.; Fassi-Fehri, O. DFT investigations of the hydrogenation effect on silicene/graphene hybrids. J. Phys. Condens. Matter. **2012**, 24, 485502. doi:10.1088/0953-8984/24/48/485502.

[5] Pujari, B. S.; Gusarov, S.; Brett, M.; Kovalenko, A. Single-side-hydrogenated graphene: Density functional theory predictions. Phys. Rev. B. **2011**, 84, 041402.

[6] Nair, R. R.; Ren, W.; Jalil, R.; Riaz, I.; Kravets, V. G.; Britnell, L.; Blake, P.; Schedin, F.; Mayorov, A. S.; Yuan, S.; Katsnelson, M. I.; Cheng, H. M.; Strupinski, W.; Bulusheva, L. G.; Okotrub, A. V.; Grigorieva, I. V.; Grigorenko, A. N.; Novoselov, K. S.; Geim, A. K. *Fluorographene: A two-dimensional counterpart of Teflon. Small. **2010**, **6**,* 2877-2884.

[7] Lew Yan Voon, L. C.; Sandberg, E.; Aga, R. S.; Farajian, A. A. Hydrogen compounds of group-IV nanosheets. Appl. Phys. Lett. **2010**, 97, 163114.

[8] Zhang, P.; Li, X. D.; Hu, C. H.; Wu, S. Q.; Zhu, Z. Z. First-principles studies of the hydrogenation effects in silicene sheets. Phys. Lett. A. **2012**, 376, 1230-1233.

[9] P, Gori.; Pulci, O.; Marsili, M.; Bechstedt, F. Side-dependent electron escape from graphene- and graphane-like SiC layers. Applied Physics Letters. **2012**, 100, 043110.

[10] Leenaerts, O.; Peelaers, H.; Hernandez-Nieves, A. D.; Partoens, B.; Peeters, F. M. First-principles investigation of graphene fluoride and graphane. Physical Review B. **2010**, 82, 195436.

DFT STUDY AND SPECTROSCOPIC ANALYSIS OF THE PESTICIDE IMAZAQUIN

R. Tazi[1,*], S. Zaydoun[2], A. Zrineh[1], M. El Azzouzi[1] and M. Benzakour[3]

[1]Laboratory of Materials, Nanomaterials and Environment. Faculty of Sciences, University Mohammed V, Rabat, Morocco

[2]Laboratory of Spectroscopy, Molecular Modeling, Materials and Environment. Faculty of Sciences, University Mohammed V, Rabat, Morocco

[3]Laboratory for Materials Engineering and Modelling. Faculty of Sciences, Dhar El Mahraz, University Sidi Mohammed Ben Abdellah, Fez, Morocco

*Corresponding author email: rabeatazi@hotmail.com

Abstract: Our work is a theoretical study of energy and structural characteristics concerning the interaction sites of the Imazaquin with water to develop correlations between calculations and experience. To determine the fate of the plant protection product in environment, it is essential to understand its behavior and its reactivity in aqueous media. Calculations of neutral and hydrated Imazaquin were conducted using the Gaussian 03 program package and Density Functional Theory calculations were used for geometry optimizations performed without restriction of symmetry. Structural and electronic properties were determined in the gas phase and in aqueous solution. The interaction sites of the pesticide with water have been studied. The vibration spectra have been determined for fully optimized structures.

Keywords: Quantum chemical calculations; Imazaquin; Aqueous media; Interaction sites.

INTRODUCTION

Imazaquin,   2-(4-Isopropyl-4-methyl-5-oxo-4,5-dihydro-1H-imidazol-2-yl)-3-quinoline carboxylic acid (Figure 1), is a broad-spectrum imidazolinone herbicide used for the protection of variety of agricultural products and constitutes an important environmental pollutant [1,2].

To determine the fate of the plant protection product and to have detailed information about this compound that comes in contact with the soil, it is important to understand its reactivity in aqueous solution [3,4].

In the present work, ab-initio calculations were conducted to determine the structural characteristics and interaction sites of Imazaquin with water to establish correlations between the calculations and the experience.
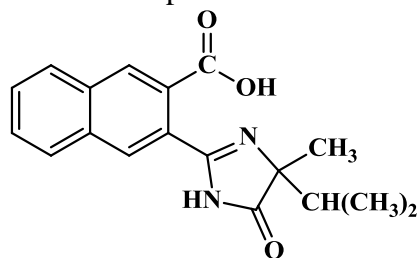

Figure 1. Structure of Imazaquin

METHODS AND MATERIALS

Study of neutral and hydrated Imazaquin was carried out with the Density Functional Theory (DFT) [5-7,]. The functional hybrid B3LYP coupled to the basis set 3-21G [8] has been used for geometry optimizations performed without restriction of symmetry with the Gaussian 03 package [9]. The stationary points of optimized minima structures were examined by frequency calculations and showed zero negative frequencies. Vibrational frequencies were analytically determined for fully optimized structures. All the geometries of the calculated electronic structures were visualized by the Gaussview program [10].

RESULTS AND DISCUSSION

Structure

In our case, three isomers of hydrated compounds have been determined. Optimized structures are presented in Figure 2 and Table 1. Values of dihedral angles reveal that the molecular structure has a non-planar conformation which indicates an angle of 14.9°. The hydrolysis has no effect on the overall geometry of the pesticide. The comparison between hydrogen bonds (O-H…O) values for the three hydrated forms shows that hydr1 is the most stable but gives stability by the formation of OH---OH$_2$ bond.

| Imazaquin | Imazaquin hydr1 | Imazaquin hydr2 | Imazaquin hydr3 |
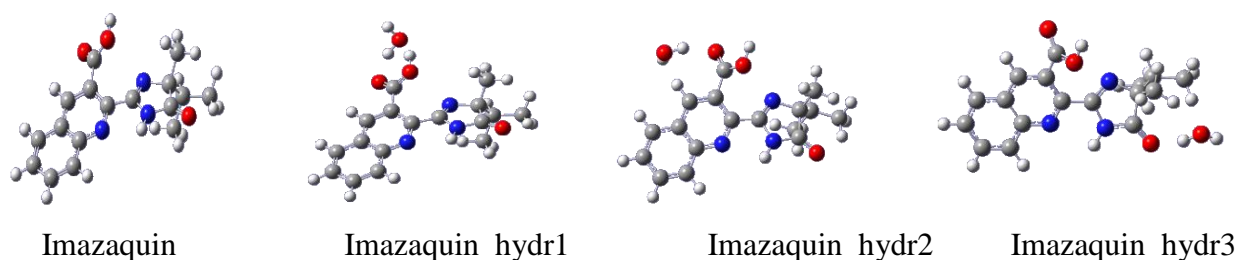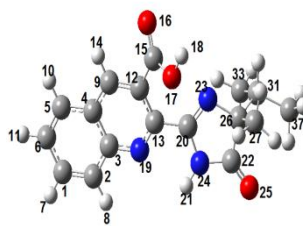
Figure 2. Calculated molecular conformations

Table 1. Geometrical parameters (distances R in Å, angles A and dihedral angles D in °)

	NEUTRAL	IMAZAQUIN		
		HYDRATED		
		H$_{18}$ hydr1	O$_{16}$ hydr2	O$_{25}$ hydr3
R(C$_{15}$,O$_{16}$)	1.227	1.260	1.238	1.228
R(C$_{15}$,O$_{17}$)	1.371	1.330	1.363	1.369
R(O$_{17}$,H$_{18}$)	0.996	1.073	0.997	0.997
R(C$_{12}$,C$_{15}$)	1.489	1.490	1.484	1.489
R(C$_{12}$,C$_{13}$)	1.426	1.427	1.428	1.427
R(C$_{13}$,N$_{19}$)	1.330	1.330	1.328	1.331
R(C$_{13}$,C$_{20}$)	1.472	1.472	1.472	1.471
R(C$_{20}$,N$_{23}$)	1.293	1.292	1.293	1.290
R(C$_{20}$,N$_{24}$)	1.403	1.404	1.402	1.411
R(N$_{24}$,C$_{22}$)	1.393	1.392	1.393	1.377

R(C_{22},O_{25})	1.233	1.233	1.233	1.244
R(C_{22},C_{26})	1.553	1.553	1.553	1.551
R(C_{26},N_{23})	1.509	1.508	1.509	1.511
R(H_{18},OH_2)	-	1.482	-	-
R(O_{16},HOH)	-	-	1.781	-
R(O_{25},HOH)	-	-	-	1.713
A(C_{15},C_{12},C_{13})	125.98	126.01	124.35	126.17
A(O_{16},C_{15},C_{12})	124.64	120.70	126.00	124.51
A(O_{16},C_{15},O_{17})	123.46	123.55	121.56	123.61
A(C_{15},O_{17},H_{18})	108.53	107.81	108.81	108.84
A(C_{20},N_{23},C_{26})	106.28	106.29	106.27	106.80
A(N_{23},C_{20},N_{24})	115.34	115.30	115.36	114.71
A(N_{24},C_{22},O_{25})	127.17	127.11	128.78	125.48
A(O_{25},C_{22},C_{26})	128.79	128.85	115.358	129.74
A(O_{17},H_{18},OH2)	-	154.21	-	-
A(C_{15},O_{16},HOH)	-	-	124.60	-
A(C_{22},O_{25},HOH)	-	-	-	119.18
D(O_{16},C_{15},C_{12},C_9)	-36.02	-31.42	-35.61	-34.45
D(C_{12},C_{15},O_{17},H_{18})	176.42	-179.19	177.08	175.94
D(C_{15},C_{12},C_{13},C_{20})	-14.93	-17.61	179.95	-14.83
D(C_{20},N_{24},C_{22},O_{25})	-178.83	-178.65	-178.80	179.85
D(C_{13},C_{20},N_{23},C_{26})	-177.22	-177.26	-176.57	-176.16
D(C_{15},O_{17},H_{18},OH2)	-	7.75	-	-
D(C_{12},C_{15},O_{16},HOH)	-	-	35.15	-
D(N_{24},C_{22},O_{25},HOH)	-	-	-	24.29

Energy

The energies and dipolar moments were calculated in gas phase and presented in Table 2.

Table 2. Energies and dipolar moments values

Form	Imazaquin	Imazaquin hydrated		
		Imazaquin hydr1	Imazaquin hydr2	Imazaquin hydr3
E_T (u.a)	-1042.247074	-1118.267661	-1118.252384	- 1118.2494802
dipolar moment (Debye)	4.1899	6.0490	5.2992	5.1922

It is noteworthy that the Imazaquin is essentially stable to hydrolysis. As concluded from structural data, Imazaquin hydr1 is energetically more stable than the others and hydration is favorable to the carboxylic acid function group who easily loses an hydrogen.

Partial charges on atoms

Partial charges are introduced due to the asymmetric distribution of electrons in chemical bonds between atoms with different electronegativity. The molecule contains several sites likely to be ionized. The result from charge calculations are presented in Table 3.

Table 3. Charges values for the computed structures

Charge	Imazaquin	Imazaquin hydrated		
		hydr1	hydr2	hydr3
$qH_{18\_}$	0.371	0.381	0.376	0.373
qO_{17}	- 0.543	-0.505	-0.535	-0.545
qO_{16}	- 0.480	-0.541	-0.511	-0.481
qO_{25}	- 0.499	-0.585	-0.498	-0.531
qN_{23}	- 0.511	-0.499	-0.516	-0.503
qN_{24}	- 0.767	-0.698	-0.701	-0.701
qN_{19}	- 0.701	-0.766	-0.767	-0.767
qH_{21}	0.344	0.342	0.345	0.318

The results obtained show that the positive charge on the hydrogen atom from the OH group indicates its ability to form a bond with H_2O. This confirms the previous results.

Distribution of frontier orbitals

The gap Δ, difference in energy between the HOMO and LUMO, is an indicator of stability in a molecule, indeed more the gap is large and more stability of the molecule is great. The energy gap for the different possible conformers was calculated to compare the chemical activity. The results are presented in the Table 4.

Table 4. Orbital energies in u.a

	Imazaquin neutral	Imazaquin hydrated		
		hydr1	hydr2	hydr3
HOMO	-0.22987	-0.22433	-0.23165	-0.23814
LUMO	-0.08010	-0.07709	-0.07734	-0.08287
Δ	0.14977	0.14724	0.15431	0.15527

Our results indicate that the form hydr1 will likely be more susceptible to further reaction because of the smaller HOMO-LUMO gap.

IR study

The spectroscopic study shows, after hydrolysis in position 1 (hydr1) of the neutral form, there is loss of the characteristic band for the link OH (3490.23 cm^{-1}). This is in agreement with the formation of H_3O^+ by transfer of H from COOH to H_2O. In an aqueous medium, it seems that the Imazaquin exists probably as an anionic form which would be degraded by photolysis.
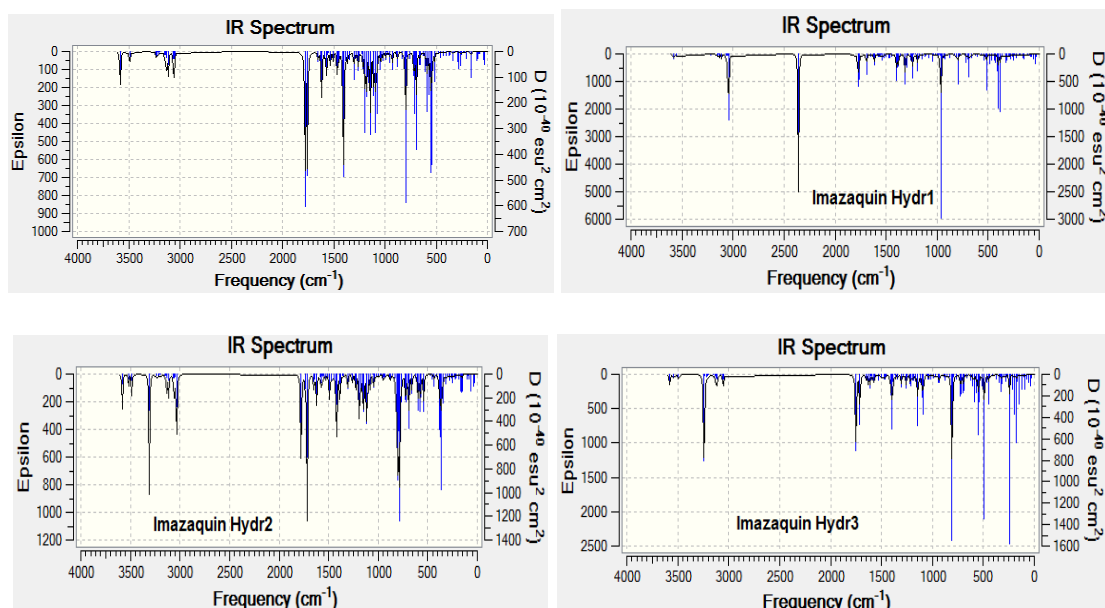
Figure 4. Neutral and hydrated Imazaquin IR spectra

CONCLUSION

DFT calculations allowed us to determine the molecular conformations of the neutral and hydrated Imazaquin and to conclude that the hydrolysis on the carboxyl group is the most favorable. Frontier orbital analysis has shown that the hydrated form is most reactive than the neutral form. The frequencies of the internal modes calculated for the neutral form and different aqueous forms showed a difference in spectra.

ACKNOWLEDGEMENTS

REFERENCES

[1] Quicke, H.E.; Hoien, E.; Beaudrot, L. *Imazaquin, Imazapic and Pendimethalin for Weed Control in Hybrid Poplar: The 1998 Clatskanie, Oregon Study*; American Cyanamid Forestry Technical Service Research Report, **1999**.

[2] Park, Y.; Sun Z.; Ayoko, G.A.; Frost, R.L. Removal of herbicides from aqueous solutions by modified forms of montmorillonite *Journal of Colloid and Interface Science* **2014**, *415*, 127-132.

[3] Garcia, J.C.; Takashima, K. Photocatalytic degradation of imazaquin in an aqueous suspension of titanium dioxide *Journal of Photochemistry and Photobiology A: Chemistry*, **2003**, *155*, 215-222.

[4] Barkani, H.; Catastini, C.; Emmelin, C.; Sarakha, M.; El Azzouzi, M.; Chovelon, J.M. Study of the phototransformation of imazaquin in aqueous solution: a kinetic approach *Journal of Photochemistry and Photobiology A: Chemistry*, **2005**, *170*, 27-35.

[5] Becke, A.D. Density functional thermochemistry. III. The role of exact exchange *J. Chem. Phys.*, **1993**, *98*, 5648-5652.

[6] Becke, A.D. Density-functional exchange-energy approximation with correct asymptotic behavior. *Phy. Rev. A*, **1988**, *38*, 3098-3100.

[7] Lee, C.; Yang, W.; Parr, R.G. Development of the Colle-Salvetti correlation energy formula into a functional of the electron density. *Phys. Rev. B*, **1988**, *3*, 785-789.

[8] Hehre, W.J.; Radom, L.; Schleyer, P.V.R.; Pople, J.A. *Ab Initio Molecular Orbital Theory*, Wiley: New York, 1986.

[9] Frisch, M.J.; Trucks, G.W.; Schlegel, H.B.; Scuseria, G.E.; Robb, M.A.; Cheeseman, J.R.; Montgomery Jr., J.A.; Vreven, T.; Kudin, K.N.; Burant, J.C.; Millam, J.M.; Iyengar, S.S.; Tomasi, J.; Barone, V.; Mennucci, B.; Cossi, M.; Scalmani, G.; Rega, N.; Petersson, G.A.; Nakatsuji, H.; Hada, M.; Ehara, M.; Toyota, K.; Fukuda, R.; Hasegawa, J.; Ishida, M.; Nakajima, T.; Honda, Y.; Kitao, O.; Nakai, H.; Klene, M.; Li, X.; Knox, J.E.; Hratchian, H.P.; Cross, J.B. ; Bakken, V.; Adamo, C.; Jaramillo, J.; Gomperts, R.; Stratmann, R.E.; Yazyev, O.; Austin, A.J.; Cammi, R.; Pomelli, C.; Ochterski, J.W.; Ayala, P.Y.; Morokuma, K.; Voth, G.A.; Salvador, P.; Dannenberg, J.J.; Zakrzewski, V.G.; Dapprich, S.; Daniels, A.D.; Strain, M.C.; Farkas, O.; Malick, D.K.; Rabuck, A.D.; Raghavachari, K.; Foresman, J.B.; Ortiz, J.V.; Cui, Q.; Baboul, A.G.; Clifford, S.; Cioslowski, J.; Stefanov, B.B.; Liu, G.; Liashenko, A.; Piskorz, P.; Komaromi, I.; Martin, R.L.; Fox, D.J.; Keith, T.; Al-Laham, M.A.; Peng, C.Y.; Nanayakkara, A.; Challacombe, M.; Gill, P.M.W.; Johnson, B.; Chen, W.; Wong, M.W.; Gonzalez, C.; Pople, J.A. *Gaussian 03, Revision D, Gaussian*, Inc., Wallingford, CT, 2004.

[10] Dennington II, R.; Keith, T.; Millam, J.; Eppinnett, K.; Hovell, W.L.; Gilliland, R. *GaussView, Version 3.0.9, Semichem* Inc., Shawnee Mission, KS, 2003**.**

AB INITIO STUDY OF THE ELECTRONIC STATES OF DIFFERENT TiN₂ ISOMERS

Zohra Guennoun[1] and Najia Komiha[2,*]

[1]Department of Chemistry, University of Basel, Switzerland
Current address: Université de Bordeaux I, Institut des Sciences Moléculaires,
351 Cours de la Libération, 33405 Talence cedex
[2] LS3ME- Equipe de Chimie Théorique et Modélisation,
Université Mohamed V, Rabat, Morocco

*Corresponding author email: komiha@fsr.ac.ma

Abstract: The ground and electronic excited states of TiN$_2$ correlating with the lowest dissociation asymptotes N$_2$ (X$^1\Sigma_g^+$) + Ti (^{3}F), N$_2$ (X$^1\Sigma_g^+$) + Ti (^{5}F), and N$_2$ (X$^1\Sigma_g^+$) + Ti (^{1}D) have been studied by full valence complete active space self-consistent field (CASSCF) and restricted coupled cluster with perturbative triples (RCCSD(T)) ab initio methods. For the bound states, equilibrium geometries, total energies, and harmonic wavenumbers are reported and compared with the experiment, where possible. The potential energy surfaces of the lowest electronic states have also been calculated. Along the dissociation path, the regions of vibronic and spin-orbit couplings have been located, the crossing between the most important states ($^5\Delta$ and $^3\Phi$) are at 2.2A.

Keywords: Electronic states; highly correlated quantum chemistry methods; potential energy curves, equilibrium geometries, excitation energies, asymptotic behaviour, harmonic wavenumbers.

INTRODUCTION

Since the past 30 years, there is ongoing interest in metal complexes which bind dinitrogen. Activation of small molecules and in particular of dinitrogen is indeed a fundamental challenge to synthetic as well as theoretical chemistry. Among metal-containing species, titanium nitrides have been the interest of many scientists especially in material sciences [1-2] due to their unique mechanical features such as self-lubricity, high wear resistance, high conductivity [3], and an extreme high melting temperature and hardness [4]. These species are generally referred to as refractory hard metals due to their unusual metallic, covalent, and ionic properties [5-6]. They have a valence band with a strong mixed p-d character as in covalent compounds and a conduction band with mainly d character as in metallic species. All these properties make these compounds very good candidates for many applications in different areas, such as in semiconductor device technology [7-8] or in surgery tools and implants [4], and also very attractive from a fundamental point of view [5]. In addition, the interaction of titanium with nitrogen is of considerable importance in catalysis [9-11].

Many experimental [12-14] and theoretical [15-20] studies have been devoted to TiN$_x$ species to understand the different coordination modes of the dinitrogen molecule to the transition metal. These studies showed that the bonding mode of N$_2$ in most cases is end-on with a linear Ti-N-N structure in which the N$_2$ molecule is very little perturbed as seen in most

of the transition metal dinitrogen complexes [21,22]. From experiments carried out in cryogenic matrices [12,14], weakly TiN_x bound complexes were observed but only after photoactivation of the Ti atoms, thus evidencing the activation of the N–N triple bond by transition metals. The N-N bond distance is within 0.02 Å , the free nitrogen molecule (1.10 Å), and the N-N stretch frequency is shifted to lower values compared to the free N_2 (2331 cm^{-1}, from our calculations and [35]), down to about 2000 cm^{-1} when bounded. Side-bound TiN_2 species (cyclic and bent structures) were also observed and characterized in the matrix infrared studies [14].

In the present study, our motivation stems from the general interest in M-N_2 interactions especially in the case of TiN_2. This species, even though seems simple, it exhibits several electronic states with different structures having similar energies. In what follows, the ground and low-lying excited states of TiN_2 have been investigated and the results compared to reported experimental and theoretical data. The calculations have been performed using the complete active space self-consistent field (CASSCF) method for the vertical excitation energies and restricted coupled cluster with perturbative triples (RCCSD(T)) *ab initio* approach for the optimization of the structures and the mapping of the potential energy curves. For selected states, potential energy surfaces have also been computed with respect to the Ti + N_2 (X $^1\Sigma_g^+$) asymptote. The three states studied here are the lowest quintet ($^5\Delta$), triplet ($^3\Phi$) and singlet ($^1\Sigma$). They dissociate towards three close-lying asymptotes Ti + N_2 X $^1\Sigma_g^+$) with Ti having either a ^3F (Ti ground state term ($4s^23d^2$) [1]), ^5F ($\approx$ 6557 cm^{-1} above) or ^1D state symmetry (lying $\approx$ 7255 cm^{-1} above the ground state, Table 1). The lowest excited state of N_2 ($^3\Sigma_u^+$) is 49754 cm^{-1} above the ground state [24], which is too high to be considered here as a dissociative product.

Table 1. Lowest asymptotes. The experimental relative energies are taken from (a): [23,35] and (b): [24].

Titanium + N_2	States		Relative energy (cm^{-1})	
			Experimental	Our RCCSD(T) calculations
a^{3}F +	X$^1\Sigma_g^+$ $\longrightarrow$	$^3\Sigma + {}^3\Pi + {}^3\Delta + {}^3\Phi$	0.0$^{(a)}$	0.0
^{5}F +	X$^1\Sigma_g^+$ $\longrightarrow$	$^5\Sigma + {}^5\Pi + {}^5\Delta + {}^5\Phi$	6556.8$^{(a)}$	9889.0
^{1}D +	X$^1\Sigma_g^+$ $\longrightarrow$	$^1\Sigma + {}^1\Pi + {}^1$c	7255.3$^{(a)}$	10292.4
^{3}P +	X$^1\Sigma_g^+$ $\longrightarrow$	$^3\Sigma + {}^3\Pi$	8436.6$^{(a)}$	
b^{3}F +	X$^1\Sigma_g^+$ $\longrightarrow$	$^3\Sigma + {}^3\Pi + {}^3\Delta + {}^3\Phi$	11531.8$^{(a)}$	
^{1}G +	X$^1\Sigma_g^+$ $\longrightarrow$	$^1\Sigma + {}^1\Pi + {}^1\Delta + {}^1\Phi + {}^1\Gamma$	12118.4$^{(a)}$	
a^{3}F +	A$^3\Sigma_u$ $\longrightarrow$	$^{5,3,1}\Sigma + {}^{5,3,1}\Pi + {}^{5,3,1}\Delta + {}^{5,3,1}\Phi$	49754.0$^{(b)}$	
a^{3}F +	B$^3\Pi_g$ $\longrightarrow$	$^{5,3,1}\Sigma + {}^{5,3,1}\Pi + {}^{5,3,1}\Delta + {}^{5,3,1}\Phi + {}^{5,3,1}\Gamma$		
a^{3}F +	C$^3\Pi_u$ $\longrightarrow$	$^{5,3,1}\Sigma + {}^{5,3,1}\Pi + {}^{5,3,1}\Delta + {}^{5,3,1}\Phi + {}^{5,3,1}\Gamma$		

RESULTS AND DISCUSSION

Computational details

The full valence state-averaged CASSCF [25,26] and restricted coupled cluster with perturbative triples (RCCSD(T)) approaches [27,28] have been used to describe all the electronic states correlating with the lowest Ti + N_2 asymptotes (Table 1). The single and

double excitations out of the CASSCF reference functions include all valence electrons of TiN_2 species, i.e., 14. To define the active space, all possible molecular orbitals initially made from $4s$ and $3d$ atomic orbitals of titanium and $2p$ atomic orbitals of nitrogen atoms were included. The number of configuration state functions generated in CASSCF was about 10^6 for the different TiN_2 structures studied in this work. The standard correlation consistent aug-cc-pVTZ (AVTZ) and aug-cc-pVQZ (AVQZ) basis sets of Dunning [12,13] have been employed, and all the computations have been performed with the MOLPRO quantum chemistry package [31].

Calculations have been performed for three different coordination modes of N_2 to titanium: a linear structure Ti-N-N, a cyclic one $Ti(N_2)$, and a T-shaped conformation (NTiN), as seen in Figure 1. For each isomer, three different spin states (singlet, triplet, and quintet) have been investigated. The type of bonding for the different states will be discussed in terms of electronic structures, total energies, bond distances, and vibrational frequencies (see Table 2).

Table 2. Optimized (RCCSD(T) / VTZ) cyclic, bent and linear states of TiN_2 for different multiplicities. The frequencies are given in cm^{-1}.

	Energy (a.u.)	Ti-N (Å)	N-N(Å)	TiNN (degrees)
NTiN cyclic ($^1A_1$)	-957.797554	1.792	1.394	67.14
	[590.0 **(a′)**; 595.91 **(a′)**; 1023.57 **(a′)**]			
NTiN cyclic ($^3B_1$)	-957.821713	1.991	1.214	72.40
TiN_2 cyclic ($^5B_1$)	-957.814810	2.204	1.162	74.68
	Energy (a.u.)	Ti-N (Å)	Ti-N (Å)	NTiN (degrees)
NTiN bent ($^5A_1$)	-957.654178	1.863	1.863	101.20
	[185.45 (a1); 509.52 (b2); 701.16 (a1)]			
NTiN bent ($^5A_2$)	-957.632902	1.829	1.829	79.89
NTiN bent ($^1A_1$)	-957.797554	1.792	1.792	45.78
NTiN bent (3A')	-957.719576	1.613	2.903	36.67
NTiN bent ($^3A_2$)	-957.708743	1.760	1.760	122.30
NTiN bent ($^3B_2$)	-957.654589	1.811	1.811	114. 00
	Energy (a.u.)	Ti-N (Å)	N-N (Å)	TiNN (degrees)
TiN_2 linear ($^1\Sigma$)	-957.788484	1.990	1.131	180.00
	[212.14 (b1); 298.45 (b2); 338.66 (a1); 1862.40 (a1)]			
TiN_2 linear ($^3\Sigma$)	-957.835097	4.553	1.104	180.00
TiN_2 linear ($^3\Phi$)	-957.792657	1.966	1.149	180.00
TiN_2 linear ($^5\Delta$)	-957.823033	2.014	1.136	180.00
	[276.03 (π); 385.92 (σ); 1935.06 (σ)]			

Vertical excitation energies for the investigated systems have also been computed at the correlated level and summarized in Table 3.

Table 3. CASSCF state averaged/AVQZ calculations of the electronic states at the RCCSD(T) optimized geometry of TiN_2.

Excitation energies (eV)		C.I. coefficients	Wavefunctions						
			Occupation numbers						Lz^2
			σ_{sTi} δ_{3dz^2Ti} $\delta_{3dx^2-y^2Ti}$ δ_{3dxyTi} δ_{3dyzTi} δ_{3dxyTi}						
$^5\Delta$	0.000	0.9376140	a	0	0	a	a	a	4.00
$^3\Phi$	0.484	0.6451993	2	a	0	a	0	0	8.99
		0.5491833	2	0	0	0	a	a	
$^5\Pi$	0.569	0.4189479	a	a	a	a	0	0	1.00
		-0.6776651	a	0	a	0	a	a	
		0.5111261	a	a	0	0	a	a	
$^5\Phi$	0.579	0.7067554	a	a	a	a	0	0	8.99
		-0.6392874	a	0	a	0	a	a	
$^3\Sigma$	0.702	0.4339115	2	0	0	a	a	0	0.00
		0.2715777	2		a				
$^3\Delta$	0.716	0.7977312	b	0	0	a	a	a	4.00
$^3\Pi$	0.797	-0.5064044	2	a	0	a	0	0	1.01
		0.5947511	2	0	0	0	a	a	
$^3\Gamma$	1.298	0.4803454	a	0	0	a	b	a	15.97
		-0.4667351	a	0	0	b	a	a	
		0.4713362	a	a	0	0	2	0	
		-0.4564068	a	a	0	2	0	0	
$^1\Sigma$	1.420	0.4339115	2	0	0	0	2	0	0.00
		0.2715777	2	0	0	2	0	0	
		-0.2767567							
		-0.2733388							
$^1\Pi$	1.453	0.40000154	2	a	0	b	0	0	1.00
		-0.40000154	2	0	0	0	b	a	

Reference energy -957.504953 a.u., core configuration: $\sigma^2_{2sN2}\sigma^{*2}_{2sN2}\sigma^2_{2pzN2}\pi^2_{2pxN2}\pi^2_{2PyN2}$

Electronic states

Geometry optimizations

The geometry optimizations have been performed using the RCCSD(T)/AVTZ level of calculation. The approach of N_2 in an axial geometry to the ground ^3F state of Ti gives rise to four electronic states: $^3\Sigma$, $^3\Pi$, $^3\Delta$, and $^3\Phi$, which are all repulsive. The lowest linear state correlating to the first excited state of Ti (^5F) + N_2 (X $^1\Sigma g^+$) leads to a $^5\Delta$ symmetry state. This state corresponds to a minimum, as seen in Table 3, with R_{Ti-N} = 2.014 Å and R_{N-N} = 1.136 Å. These values are in good agreement with the values found from DFT calculations (R_{Ti-N} = 1.965 Å and R_{N-N} = 1.158 Å in [14], R_{Ti-N} = 2.009 Å and R_{N-N} = 1.124 Å in [32]) and those obtained by Kardahakis et al. from different *ab initio* methods [19]. According to our calculations, this state is a minimum with real vibrational frequencies (Table 2). The σ symmetry frequency, assigned to the N-N stretching vibrational mode, is calculated to lie at 1935 cm^{-1} which is close to the DFT value reported by Kushto et al. [14] at 1941 cm^{-1}, and to the experimental ones at 1847.1 and 1847.0 cm^{-1} reported in [12] and [14] respectively from matrix infrared spectroscopy of laser-ablated titanium with nitrogen reaction products.

From the data reported in Table 2, it is worth noting that the geometry optimization of the linear structures give a $^3\Sigma$ state, lower in energy than the $^5\Delta$, but the $^3\Sigma$ minimum shows a large Ti-N distance (4.553 Å). Hence, this structure is a Van Der Waals complex of a dissociative state as no real harmonic frequency has been obtained. As observed for all group IV metals [12,14,33,34], the end-bound TiN$_2$ isomer ($^5\Delta$ symmetry, Figure 1) corresponds to the global minimum in agreement with previous theoretical studies [14-19,32]. The linear $^3\Phi$ state is higher in energy with a structure close to the ground state one. However, no real harmonic frequency has been found. This state may be a saddle point in the potential energy surface due to an avoided crossing. The $^1\Sigma$ state is also calculated to be a minimum with the following harmonic wave numbers: 212.14, 298.45, 338.66 cm^{-1} (spectral region not studied experimentally) and 1862.40 cm^{-1} in agreement with the experimental data at 1847.1 in [12] and 1847.0 in [14]. All bound molecular states correlate to the first excited states of Ti (^{5}F or ^{1}D) as reported in Tables 1 and 4. The bonding in the linear TiN$_2$ species is due to a sigma charge donation from N$_2$ to Ti, with a Ti to N$_2$ "back donation" through the pi-conjugated system.
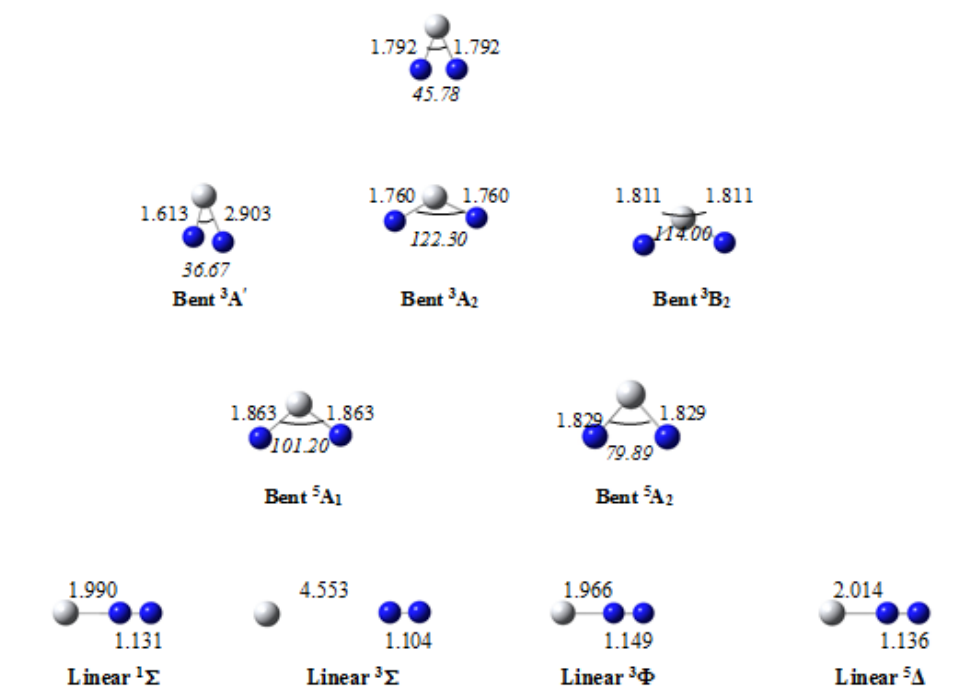

Figure 1. Optimized structures of the electronic states investigated for TiN$_2$. The lengths are given in Å and the angles (italic characters) in degrees.

The cyclic and bent structures have also been investigated in this study. The only states with real harmonic wave numbers are found to be:
- the cyclic ^{1}A$_1$ state with the strongest infrared absorption band predicted to be the Ti-N stretching and to lie at 1023.57 cm^{-1}. This is in a reasonable agreement with the band observed in the cryogenic matrix experiments at 1125.9 cm^{-1} [14] (isotopic effects are not taken into account here). The other two computed values (590.0 and 595.91 cm^{-1}) for the cyclic ^{1}A$_1$ state are out of the spectral region studied experimentally in [12,14]. Among the cyclic optimized structures, the ^{1}A$_1$ state is the highest in energy and is characterized by a strong Ti-N and a long N-N bond lengths, as found in [14]. However, from our study the cyclic ^{3}B$_1$ state is found to be the lowest

in energy while it is predicted to be a $^3A_2$ from DFT calculations conducted by Kushto and co-workers [14];

- the bent $^5A_1$ quintet state has the following frequencies: 185.45, 509.52 and 701.16 cm^{-1}, which are also out of the spectral ranges within investigated [12,14]. The calculated frequencies for other bent structures by Kushto et al.[14] are in the same range of the obtained values. These two bound states correlate to the linear bound ones $^5\Delta$ and $^1\Sigma$ when bending. For the T-shaped molecular systems, the bonding can be attributed to 3d (Ti)-2p(N-N) interactions in the plane of the molecule.

Vertical excitation energies

The vertical excitation energies have been calculated at the RCCSD(T)/AVTZ optimized geometry of the ground state. States averaged CASSCF calculations for the lowest states have been conducted; the results are given in Table 3. These states could be properly calculated with the right Lz angular momentum values, as seen in this table. The main configurations with the CI coefficients are also reported. It appears that the ground state $^5\Delta$ is mono configurational whereas the wave functions of most of the other states are built on several configurations.

The low-lying excited states are those of high multiplicity (quintets and triplets), the singlet states are indeed higher. The analysis of the wave functions shows that these states are weakly bound as the electrons are clearly distributed on Ti and N_2 orbitals. With respect to these results, it can be suggested that the approach of Ti leads to an activation of the dinitrogen bond as the wave function of most of the electronic states are dominated by the Ti and N_2 fragment terms.

This could be expected as N_2 is a closed shell strongly bound molecule. The axial approach of an excited Ti atom weakly changes the behavior of N_2. The harmonic wave number of the $^5\Delta$ ground state (1935 cm^{-1}) is indeed not far from(2300 cm^{-1}) which is the value of the isolated N_2 molecule.
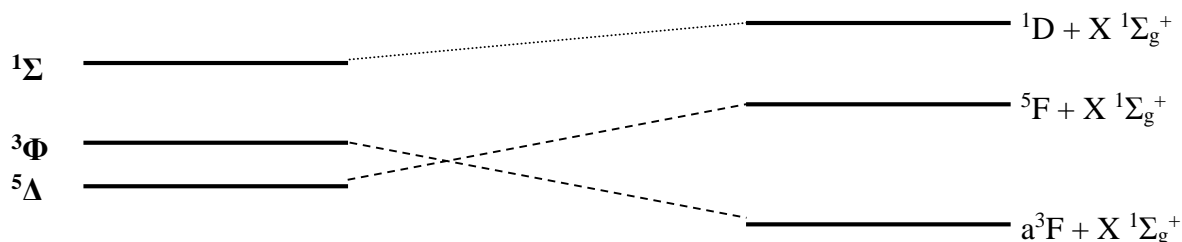
The lowest triplet state is $^3\Phi$ lying at 0.484 eV above the ground state. The lowest singlet is $^1\Sigma$ state at 1.420 eV above the $^5\Delta$ state. We notice that there are many states close in energy, this complicates their study and particularly the mapping of the potential energy curves because of all their possible couplings and mixing.

Asymptotic behaviour and potential energy curves

As the ground state is a quintet, the lowest possible correlated asymptote is Ti (^5F) + N_2 (X $^1\Sigma^+_g$). It can be seen from Tables 1 that the lowest excited state of N_2 (A$^3\Sigma^+_u$) lies 49754 cm^{-1} above the ground state (X$^1\Sigma^+_g$) [24], which is too high to be considered in the present study. The lowest excited states of titanium are ^3F (from $4s^23d^2$ configuration), ^5F (from $4s^13d^3$ configuration) which is more reactive and lies ≈ 6557 cm^{-1} above, and $^1D \approx 7255$ cm^{-1} above the first configuration [23,35]. The first low-lying quintet state correlates with the Ti (^5F) + N_2 (X $^1\Sigma^+_g$) asymptote, the triplet state with the Ti (^3F) + N_2 (X $^1\Sigma^+_g$) one, and the singlet state with the Ti (^1D) + N_2 (X $^1\Sigma^+_g$) asymptote (Table 4).

Table 4. Calculated energy of the asymptotes and correlations with lowest states of TiN_2.

Titanium + N_2	Energies RCCSD(T)/VQZ (a.u.)
$a^3F + X\ ^1\Sigma_g^+$	-957.869531
$^5F + X\ ^1\Sigma_g^+$	-957.824471
$^1D + X\ ^1\Sigma_g^+$	-957.822636
$TiN_2\ (^5\Delta)$	-957.857055
$TiN_2\ (^3\Phi)$	-957.848575
$TiN_2\ (^1\Sigma)$	-957.822659

The potential energy curves of the lowest quintet, triplet, and singlet states have been calculated at the RCCSD(T)/AVQZ level (Figure 2). These states clearly correlate with the three lowest asymptotes. The triplet state is found to be dissociative while the quintet and singlet states are bound. The binding energy is computed to be 14 kcal.mol^{-1} for the $^5\Delta$ state in agreement with the value obtained by Kardahakis et al. (13.8 kcal.mol^{-1}) [19] but lower than the one reported by Pilme et al. (30 kcal.mol^{-1}) [32]. For the $^1\Sigma$ state the binding energy is much smaller (around 4 kcal.mol^{-1}). The crossing of the $^5\Delta$ and $^3\Phi$ potential energy curves occurs at 2.2 Å. It is worthwhile to note that from the calculations performed by Kardahakis [19] the triplet state is found to be of $^3\Delta$ symmetry while the $^3\Phi$ is calculated to be the lowest in our work.
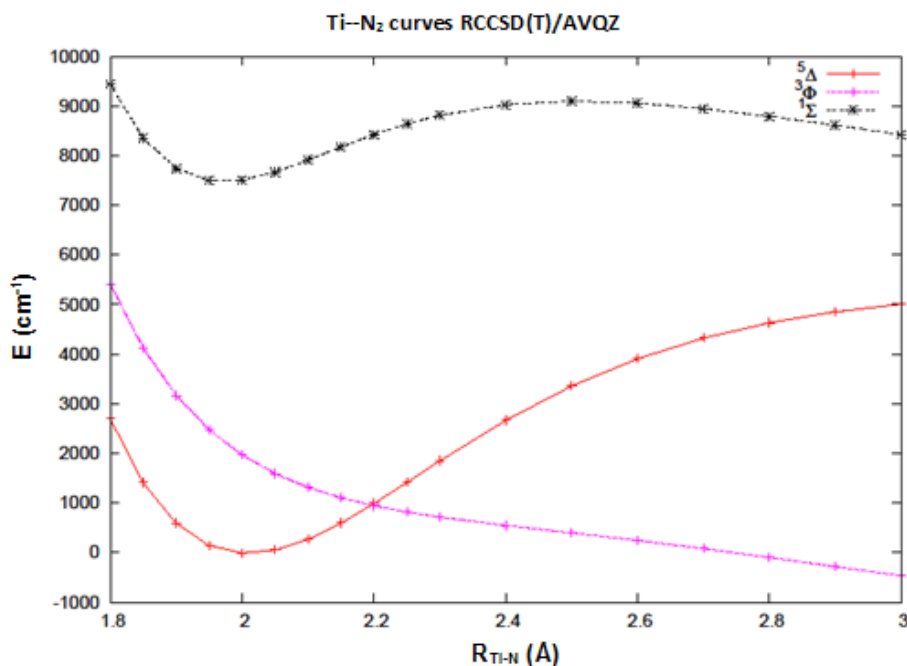
Figure 2. Potential energy curves calculated at the RCCSD(T)/AVQZ level of theory for an axial reaction approach of Ti---N_2.

CONCLUDING REMARKS

In this work, all the possible coordination of molecular N_2 to titanium have been investigated and the structures optimized. Their vertical excitation energies have also been calculated. The potential energy curves (Franck Condon region) relevant for a Ti + N_2 reaction in a linear approach have been explored for the $^5\Delta$, $^3\Phi$, and $^1\Sigma$ states. The quintet and the singlet are found to be bound while the triplet one to cross the ground state at 2.2 Å.

The ground state is calculated to possess a $^5\Delta$ symmetry in agreement with all previous studies, but the dissociative triplet state determined to be a $^3\Phi$ in our study is reported as a $^3\Delta$ in the work of Kardahakis et al. [19]. According to our results, the latter state lies much higher in energy.

An attractive potential energy curve corresponding to a state of a$^1\Sigma$ symmetry lies above with a bonding energy of ≈ 4 kcal.mol^{-1}. This state is the lowest state dissociating towards the Ti (^{1}D) + N_2 (X $^1\Sigma^+_g$) asymptote.

More states of the same symmetry and multiplicity have to be calculated with multi configurational reference methods but the problem is numerically complicated due to the metal 3d orbitals, the strong mixing and the close vicinity of the states, and the dissociation asymptotes.

Our future work is twofold: i) to explore the asymptotic region where the mixing is stronger, and ii) to study the bending of the molecule and the spin-orbit couplings.

ACKNOWLEDGEMENTS

REFERENCES

[1] Oyama, S. T. The Chemistry of Transition Metal Carbides and Nitrides; Oyama, S. T., Ed.; Blakie Academic and Professional: London, 1996; Chapter 1.

[2] Pierson, H. A. Handbbok of Refractory Carbides and Nitrides; Noyes: Westwood, NJ, 1996; Chapters 9-13.

[3] Weiller, B. H. *J. Am. Chem. Soc.* **1996**, *118*, 4975.

[4] Piscanec, S.; Ciacchi, L. C.; Vesselli, E.; Cornelli, G.; Sbaizero, O.; Meriani, S.; de Vita, A. *Acta Mater.* **2004**, *52*, 1237.

[5] Toth, L. E., Transition Metal Carbides and Nitrides; Academic Press: New York, 1971.

[6] Sundgren, J. E. *Thin Solid Films* **1985**, *128*, 21.

[7] Patsalas, P.; Charitidis, C.; Logothetidis, S.; Dimitriadis, C. A.; Valassiades, O. *J. Appl. Phys.* **1999**, *86*, 5292.

[8] Adachi, S.; Takahashi, M. *J. Appl. Phys.* **2000**, *87*, 1264.

[9] Neylon, M. K.; Bej, S. K.; Bernnet, C. A.; Thompson, L. T. *Appl.Catal., A* **2002**, *232*, 13.

[10] Shi, C.; Zhu, A. M.; Yang, X. F.; Au, C. T. *Appl. Catal. A: Gen* **2004**, *276*, 223.

[11] Kaskel, S.; Schlichte, K.; Chaplais, G.; Khanna, M. *J. Mater. Chem.* **2003**, *13*, 1496.

[12] Chertihin, G. V. and Andrews, L. *J. Phys. Chem.*, **1994**, *98*, 5891.

[13] Benhamida , M.; Meddour, A.; Zerkout, S.; Achour, S. *J. Mol. Struc.: Theochem* **2006**, *777*, 41.

[14] 1) Kushto, G. P.; Souter, P. F.; Chertihin, G. V.; Andrews, L. *J. Chem. Phys.*, **1999**, *110*, 9020.

2) Shin, S.K.; Jeong, D.W.; Kim, K. K.; Roy, M.; Park, S. M.; *Bull. Korean Chem.Soc*, **2014**, 35(2), 347

[15] Siegbahn, Per E. M. *J. Chem. Phys.*, **1991**, *95*, 364.

[16] Harrison, J. F. *J. Phys. Chem.*, *1996*, *100*, 3515.

[17] Marlo, M. and Milman, V. *Phys. Rev. B*, **2000**, *62*, 2899.

[18] Bae, Y-C; Osanai, H.; Ohno, K.; Sluiter, M.; Kawazoe, Y. *Mater. Trans.* **2002**, *43*, 482.

[19] Kardahakis, S. ; Koukounas, C.; Mavridis, A. *J. Chem. Phys.*, **2006**, *124*, 104306.

[20] Graciani, J.; Fernandez Sanz, J. ; Marquez, A. M. *J. Phys. Chem. C*, **2009**, *113,* 930.

[21] R. H. Crabtree, *The Organometallic Chemistry of the Transition Metals*, 2nd ed. (Wiley, New York, 1994).

[22] F. A. Cotton and G. Wilkinson, *Advanced Inorganic Chemistry: A Comprehensive Text*, 5th ed. (Interscience, New York, 1988).

[23] Moore, C. A. *Atomic Energy Levels*, Natl. Bur. Stand. Ref. Data Ser., Natl. Bur. Stand. Circ. No 35 U.S. GPO, Washington D.C., 1971.

[24] Miller, R.E., *J. Mol. Spectrosc.* **1966**, *19*, 185.

[25] Werner, H. J. and Knowles, P. J. *J. Chem. Phys.*, **1985**, *82*, 5053.

[26] Werner, H. J. and Knowles, P. J. *J. Chem. Phys.*, **1985**, *115*, 259.

[27] Knowles, P. J.; Hampel, C.; Werner, H. J. *J. Chem. Phys.*, **1993**, *99*, 5219.

[28] Knowles, P. J.; Hampel, C.; Werner, H. J. *J. Chem. Phys.* **2000**, *112*, 3106 (Erratum).

[29] Kendall, R. A.; Dunning Jr., T. H.; Harrison, R. J. *Chem. Phys.,* **1992**, *96*, 6796.

[30] Woon, D. E. and Dunning Jr., T. H. *J. Chem. Phys.*, **1993**, *98*, 1358.

[31] MOLPRO is a package of ab initio programs, Werner, H.-J. and Knowles, P. J. , see http://www.molpro.net.

[32] Pilme, J., Silvi, B., Alikhani, M. E. *J. Phys. Chem*. A, **2005**, *109*, 10028.

[33] Bates, J. K. and Dunn, T. M. *Can. J. Phys.*, **1976**, *54*, 1216.

[34] Bates, J. K. and Gruen, D. M. *High. Temp. Sci.*, **1978**, *18*, 27.

[35] Atomic data base, NIST; www.nist.gov